T H E U N I V E R S I T Y O F M I C H I G A N

COLLEGE OF ENGINEERING
Department of Electrical Engineering
Space Physics Research Laboratory

Final Scientific Report

MEASUREMENT OF ATMOSPHERIC PRESSURE, TEMPERATURE, AND DENSITY AT VERY HIGH ALTITUDES

A. F. Nagy
N. W. Spencer
H. B. Niemann
G. R. Carignan

ORA Projects 02804, 04004, and 04141

under contract with:

U. S. ARMY SIGNAL SUPPLY AGENCY
CONTRACT NO. DA-36-039-sc-78131
FORT MONMOUTH, NEW JERSEY

DETROIT ORDNANCE DISTRICT
BALLISTICS RESEARCH LABORATORY
CONTRACT NO. DA-20-018-509-ORD-103
DETROIT, MICHIGAN

NATIONAL AERONAUTICS AND SPACE ADMINISTRATION
CONTRACT NO. NASw-175
WASHINGTON, D.C.

administered through:

OFFICE OF RESEARCH ADMINISTRATION ANN ARBOR

August 1961

TABLE OF CONTENTS

LIST OF FIGURES

LIST OF FIGURES (Concluded)

I. INTRODUCTION

The importance of knowledge of ambient pressure, temperature, density, and composition at very high altitudes has been recognized for many years, and since 1946, a number of experiments have been carried aboard a variety of rockets to determine these physical parameters of the atmosphere. Nearly all these measurements, however, were concerned with altitudes below 90 km. Thus, until the introduction of satellites which gave results from drag measurements, only a few experiments were carried out above the 100-km level, where the mean-free path of the various gas particles is long in comparison with the dimension of the measuring device.

This report describes a research effort of the Space Physics Research Laboratory in developing a system capable of measuring atmospheric structural parameters above the 100-km level. It was decided at the start of the project that the sensors to be employed would be of the ionization gage type. The advantage of using such devices for upper-atmospheric measurements has been pointed out in an earlier work.[1] Study of the work reported in the literature also indicated that one might have a much more successful experiment if the container housing the sensors could be separated from the rocket, preferably in a degassed condition to minimize background contamination.

The general research effort was thus divided into the following tasks:

a. theoretical study of the general measurement problem;

b. development of suitable sensors;

c. development of associated electronic circuits;

d. development of a high-vacuum system to enable study and calibration of the sensors;

e. development of the nose-cone system to carry and eject the experiment.

This report describes in detail the results of these investigations, which were sponsored jointly by the U.S. Army Signal Supply Agency, the Ballistic Research Laboratory of the Aberdeen Proving Grounds, and the Goddard Space Flight Center of the National Aeronautics and Space Administration.

II. THEORETICAL STUDY

Atmospheric parameters of major interest are the pressure, density, temperature, and composition of neutral particles. These parameters are related by the ideal gas law:

$$P = R\mathbb{N}T \tag{1}$$

where

P = pressure
R = universal gas constant per molecule
$\mathbb{N}$ = number density
T = temperature

Let us consider an instrument package carrying pressure-measuring sensors moving at velocities comparable to the random thermal velocities of the constituent gases and in a region of space where the mean free path of the atmospheric molecules is large compared to the body dimensions. The sensing unit inside the body is connected to the outside atmosphere via an orifice, and an interchange of particles takes place in a manner dependent on such factors as particle velocity and density, instrument package velocity, orientation, and temperature.

It can be shown (Appendix I) that the relationship between the ambient atmospheric pressure and the pressure measured by the sensor inside the body will, under equilibrium conditions, be the thermal transpiration relation modified by a factor $f(s)$ dependent on the ratio of instrument to particle velocity. This relationship, developed variously in the literature[2,3,4] is given by Equation (2):

$$\frac{P_i}{P_o} = \left(\frac{T_i}{T_o}\right)^{1/2} f(s) \tag{2}$$

where

$f(s) = e^{-s^2} + \sqrt{\pi}\, s\, \{1 + \mathrm{erf}(s)\}$
P_o = ambient atmospheric pressure
P_i = pressure measured by sensor
T_o = ambient atmospheric temperature
T_i = temperature inside the pressure-measuring sensor
$s = \dfrac{\vec{V} \cdot \vec{x}}{U_o}$

$\vec{V}$ = instrument package velocity
$\vec{x}$ = unit vector normal to the plane of the orifice
U_o = most probable velocity of constituent ambient gas

It will be assumed that the internal temperatures are set by the wall temperature, that is, a unity accommodation coefficient will be used.[5]

Equation (2) suggests that, by placing a pressure-measuring device in a rocket-launched rolling container, a number of structural parameters can be determined if the velocity of the chamber and the relative position of the orifice are known. It is of historical interest to mention that early experiments based upon this concept were carried out using V-2 rockets as early as 1946,[3] but that no apparently good upper-atmosphere data were obtained. More recently, this method was employed successfully by Horowitz, LaGow, and others.[4,6,7]

In all these earlier experiments the sensors were mounted in the nose or the tail section of the rocket, and the outgassing from the skin of the rocket as well as the gases escaping from the rocket engine compromised very considerably the experiment at the higher altitudes.

One of the more difficult aspects of direct measurement at high altitudes is the contamination of the environment by gases originating in or on the intruding objects. Even though in certain cases "space" can be considered as a pump of very high speed, experience shows that outgassing of metallic surfaces at altitudes under consideration (above 100 km) is a relatively slow process. It was found, for example, that Sputnik III outgassed so slowly that the minimum pressure detected on its surface was only 10^{-7} mm Hg the first day, 10^{-8} mm Hg the second day, and 10^{-9} mm Hg the third day after launching. In an experiment carried by a vertical sounding rocket, there is consequently insufficient time for adequate outgassing, so it was decided that the container carrying the sensors and associated electronics should be under vacuum in the nose cone and be ejected when the altitude at which measurements are to be started is reached.

An ideally degassed rolling container moving in space, which cyclically orients the opening to the pressure-measuring device in the direction of the motion and then apposite to the direction of motion, "velocity scans" the constituent gas particles. Measurement of the resulting variation of pressure with roll angle will yield the atmospheric ambient density, pressure, and temperature. Figure 1 shows some typical pressure-versus-roll-angle variations to be expected at altitudes and velocities typical of an Aerobee 150 flight. Gage pressure readings at points displaced from the maximum pressure by 90° of roll are true ambient pressures modified by the thermal transpiration effect. Measurement of maximum and minimum gage pressure will yield ambient number density as indicated by Eqs. (3) to (6).

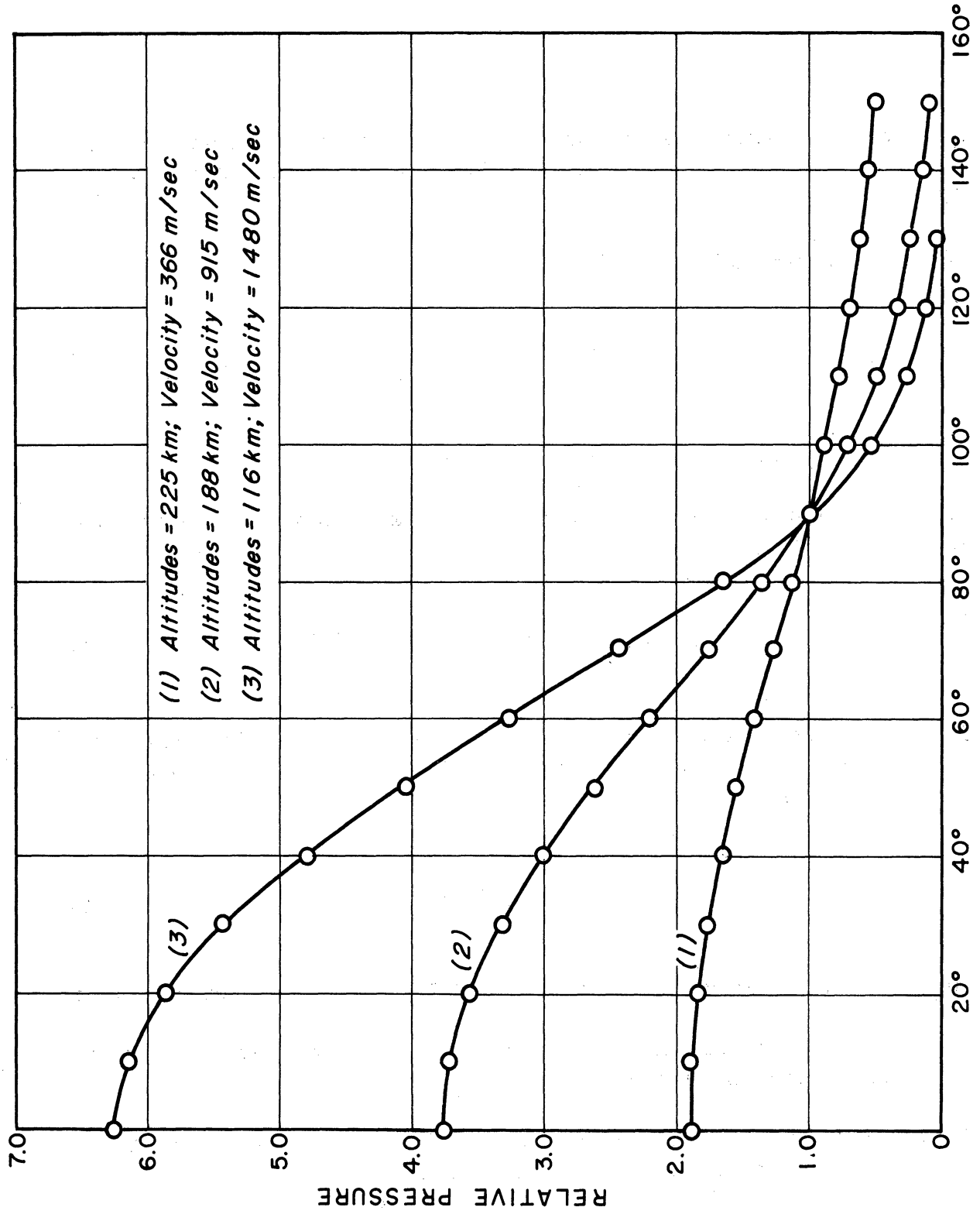

Fig. 1. Variation of relative chamber pressure with roll angle for particular velocities and altitudes typical for an Aerobee 150 flight.

From Eq. (2) we get

$$\Delta P_i = P_o \left(\frac{T_i}{T_o} \right)^{1/2} \Delta f(s) \tag{3}$$

where

$\Delta f(s)$ = change of $f(s)$ due to a change in orifice orientation,
ΔP_i = change in internal pressure corresponding to the above change in $f(s)$.

Substituting (1) into (3) and rearranging gives

$$\rho_a = \frac{\Delta P_i}{R(T_o T_i)^{1/2} \Delta f(s)} \tag{4}$$

where ρ_a = ambient atmospheric neutral gas density.

If one permits s to take on its maximum and minimum value, the corresponding change in $f(s)$ is

$$f(s_{max}) - f(s_{min}) = 2\sqrt{\pi}\, s = \Delta f^*(s) \tag{5}$$

Let ΔP_i^* be the change in gage pressure corresponding to the change in $f(s)$ indicated by (5). Substituting (5) into Eq. (4) and rearranging gives the final relation required:

$$\rho_a = \frac{\Delta P_i^*}{U_i \sqrt{\pi}\, \vec{V} \cdot \vec{x}} \tag{6}$$

where U_i = most probable velocity of gas particles inside the sensor chamber.

Equation (6) shows that the ambient density measured in this fashion does not depend on atmospheric temperature.

In most cases the minimum pressure can be neglected without significant error except near peak altitudes where the velocity of the body carrying the sensor is small. Figure 2 shows the variation of $P_{i_{max}}$, P_o and $P_{i_{min}}$ versus altitude for a hypothetical Aerobee 150 launched container. (The trajectory corresponds to Aerobee flight NN3.11F launched at Ft. Churchill, which was chosen as typical.) These curves were computed on the basis of the atmosphere having ground-level composition and the values for ambient pressure were taken

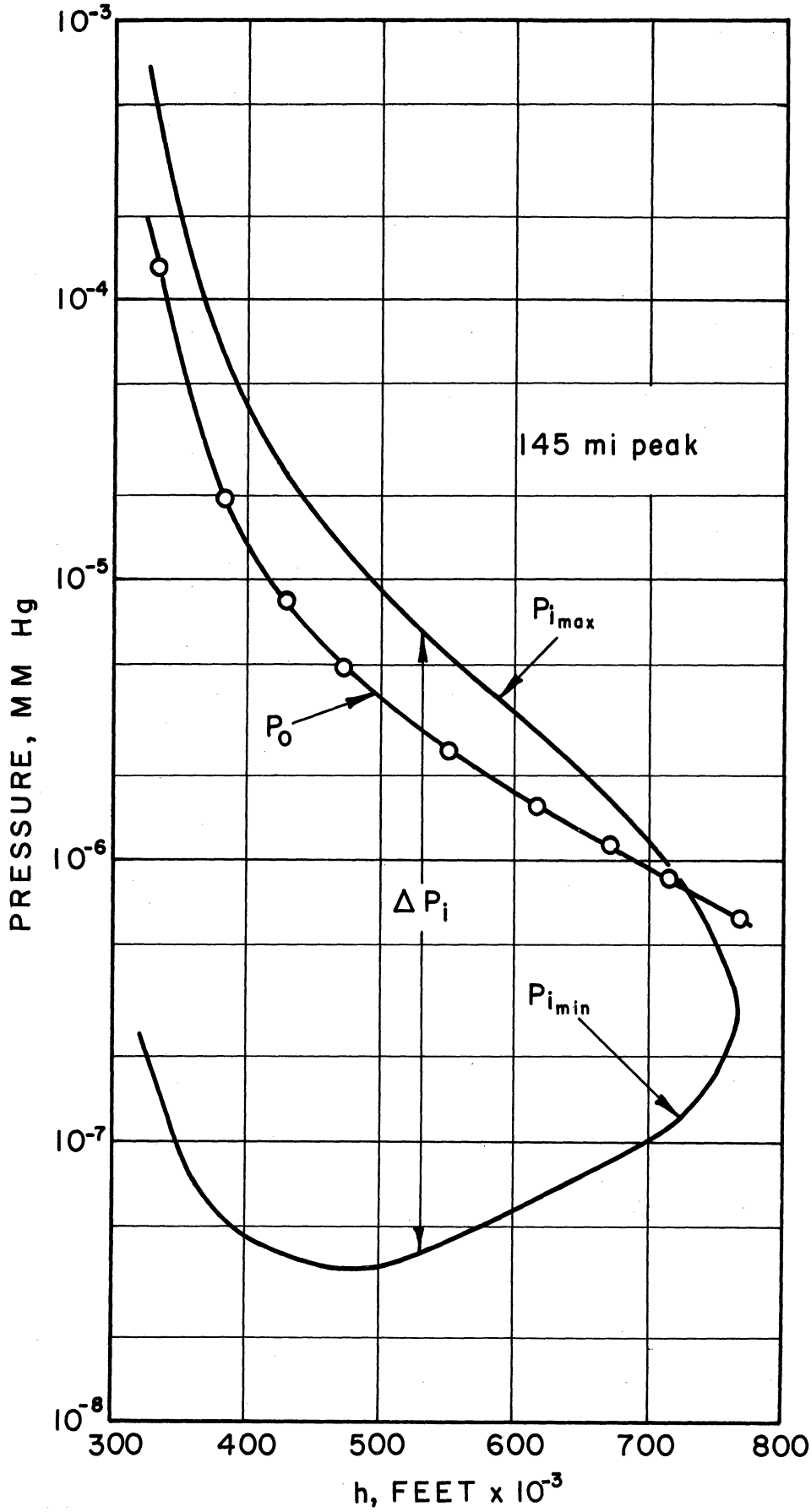

Fig. 2. Expected peressure versus altitude variation for a typical Aerobee 150 flight.

from the 1959 ARDC.

The most probable particle velocity U_i appears in both Eqs. (2) and (6), indicating that a knowledge of the mean molecular weight of the constituent gas is necessary to determine ambient pressure, temperature, and density. In earlier experiments the thermal transpiration effect was neglected in determining the ambient pressure, because at the altitudes where these measurements were made (around 100 km) this effect is small. Nevertheless, this is not the case in general, as rapidly rising ambient temperatures make the thermal transpiration effect of major importance above these altitudes. To obtain density, a mean molecular weight was usually assumed, introducing an error of the order of 10-20% at the 100- to 200-km level. This error, however, also increases as the composition of the atmosphere changes with altitude. To overcome these difficulties and to make this method of measurements useful for altitude above 100 km, the use of a partial-pressure-measuring device was proposed.[1] The use of such a sensor can establish the mean molecular weight of the gas measured; thus partial pressure, density, and temperature can be obtained. Thermal equilibrium can be assumed among the neutral gases with small error.[5] It is planned that the partial pressure sensor will measure only molecular nitrogen during the first flight. The advantages of using N_2 for measurements in the 100- to 300-km region are clear; it is the most abundant neutral gas in that region and its dissociation is probably still small at these altitudes. It should be pointed out that the use of a partial, rather than total, pressure sensor will overcome one further source of error which is due to uncertainty in atmospheric compositions. The sensitivity of devices usually employed for total pressure measurement (e.g., Philips gage, Bayard-Alpert gage, etc.) varies with change in gas composition. Ground-level compositions were usually assumed for this purpose, which admittedly introduced only a small error at low altitudes, but, of course, no such assumption is necessary when a partial pressure sensor is used.

The knowledge of the exact attitude of the container carrying the sensors is necessary for data reduction, that is, the orientation of the orifice has to be known at all times for determining $\vec{V}\cdot\vec{x}$ which appears in both Eq. (2) and (6). A number of methods for determining attitude were considered, namely, the use of magnetometers, optical sensors, gyros, and the pressure sensors themselves. Magnetometers have been used satisfactorily on a number of occasions in experiments carried out by this laboratory, so first consideration was given to this method; however, the instrumentation package will include a magnet having a field strength of approximately 2300 gauss. Thus even at points furthest from this magnet in a reasonable size package, the magnetometer would be saturated by the leakage flux. Sun and horizon detectors offer another possibility, but for simple units the data reduction is usually rather complex. The availability of miniature two-axis free gyros makes the use of such an instrument very attractive, as one gyro combined with an optical sensor will give the position of the container with respect to the velocity vector. Roll rate can be determined from the pressure variations measured by the sensors. Two pressure sensors mounted in the container as in Fig. 3 can also be used in

principle to give attitude information relative to the velocity vector.

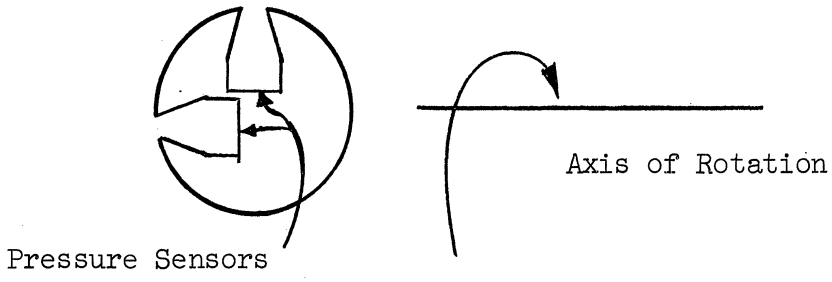

Fig. 3. Suggested mounting position of pressure sensors.

On the basis of these initial studies and considerations a general outline for the first experiment was adopted. The container will be made from stainless steel, and will be a sphere 13-in. in diameter so as to fit inside an Aerobee nose cone. This sphere will be placed in a vacuum-tight section inside the nose, which will be kept at a low pressure (10^{-5} to 10^{-6} mm Hg) by an external vucuum pump. Shortly before launching, the connections from this external pump will be removed and a 10-liters/sec ion pump mounted inside the nose cone will continue pumping the chamber until launching time. With the estimated payload, the expected peak altitude is 240 km. The 13-in. sphere will be ejected from the nose cone at an altitude of 100 km, where the ambient atmospheric pressure will be greater than the vacuum chamber pressure, thus minimizing the problems of outgassing. The sphere will carry, besides the usual amplifiers, power supplies, FM-FM transmitter, etc., the following pressure-measuring sensors:

(a) An omegatron tuned to N_2 and located on a great circle in a plane normal to the axis rotation.

(b) A Bayard-Alpert thermionic ionization gage located on the same plane as (a) but displaced from it by 120°.

(c) A Bayard-Alpert gage located at the end of the spin axis (90° from the plane of the other gages) for ambient pressure as well as attitude information.

III. SENSOR DEVELOPMENT

The omegatron was chosen as best suited for the desired measurements. It was first reported in the literature by Hipple et al.,[8] in 1949 and since then has been widely used in numerous applications. The principle of its operation has been described by several authors,[9,10,11] but for completeness it will be reviewed here briefly in a qualitative fashion. A theoretical review is given in Appendix II. Figure 4 shows the electrode arrangement of a typical

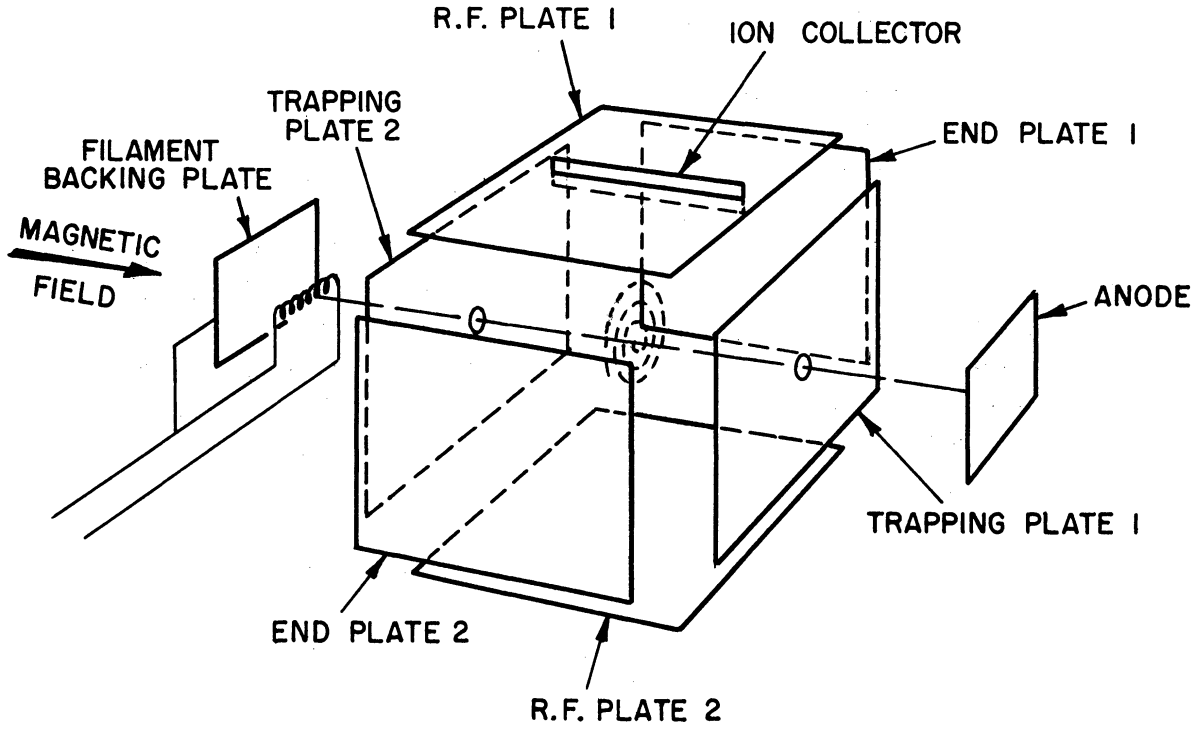

Fig. 4. Functional diagram of omegatron.

omegatron. Electrons are emitted by a thermionic cathode, and after undergoing acceleration enter into the "action volume" through a small opening. These electrons drift through this volume ionizing the gas particles present and leave through a small hole on the other side and are then collected by the anode. The rf plates provide the means of introducing an alternating electric field at right angles to the magnetic field. An ion having a given e/m ratio will describe an Archimedes spiral in a plane perpendicular to the magnetic field if the electric field has the proper angular frequency, $\omega = \frac{e}{m} B$, for the fixed magnetic flux density, B. These "resonant" ions are collected by a plate situated some distance away from the electron beam. The nonresonant ions form space charge around the electron beam. Measurement of the ion collector current versus either the frequency of the electric field or the mag-

netic field strength will give an indication of the e/m ratio and the relative abundance of the molecules of the constituent gas.

A number of simple omegatrons were built and operated before the design for the final omegatron was determined. Figure 5 shows the prototype omegatron built for flight use. The tube envelope is made an integral part of the 13-in. sphere skin. To obtain maximum conductance between the orifice and the omegatron itself, while accommodating the magnet, the chamber is oriented so as to make an angle of 45° with the normal to the orifice, as shown in Fig. 5. The plates of the omegatron are made from stainless-steel etched mesh to promote free particle movement, further improving the conductance. The various electrodes are mounted on the bottom plate which closes the chamber. A vacuum-tight seal is obtained between this plate and the envelope with an OFHC copper washer. The necessary magnetic field is provided by an Alnico permanent magnet having a field strength of approximately 2300 gauss. To minimize the problem of field alignment, a pair of soft iron polepieces are vacuum-brazed into the envelope which is made from nonmagnetic stainless steel.

The tube elements are supported by four .070-in. diameter sapphire rods which are brazed to the base plate. These rods are external to the action volume to avoid causing field perturbations. As mentioned previously, the plates are made from stainless-steel mesh. The electrons are produced by a rhenium filament supported by two glass-coated molybdenum rods as shown in Fig. 6. These rods are attached to a platinum sheet which is spot-welded to the stainless-steel mesh.

Rhenium was selected for the filament material because of its high ductility even after heating. In the early models the filament was a straight .003-in. rhenium wire, which, to prevent sagging, had to be mounted under tension. This in turn caused it to break easily when heated. On later versions the filament was made from .003-in. rhenium wire wound into a helix having a .010-in. diameter and a pitch of 150 turns/inch as shown in Fig. 6. A number of different glasses were tried for coating the molybdenum rods supporting the filament and anode. Corning No. 1720 was finally adopted as it keeps the electrical leakage resistance above the $10^{11}\Omega$ region.

As discussed earlier, the electrons are accelerated into the action volume through a .030-in. opening and after passing through a .045-in. hole on the other side are collected by the anode, a small, square platinum sheet supported in the same fashion as the filament. The ion collector is a thin strip of platinum mounted parallel to the electron beam, close to the lower rf plate, as shown in Fig. 5. It is spot-welded to the center lead of the nonmagnetic ceramic feed-through, which is intended to permit baking of the complete omegatron to a temperature of about 300-400°C.

Like all other rocket-borne devices, the omegatron must be capable of withstanding large accelerations. The prototype model was subjected to sinusoidal accelerations up to 25 g's along all the major axes without showing any

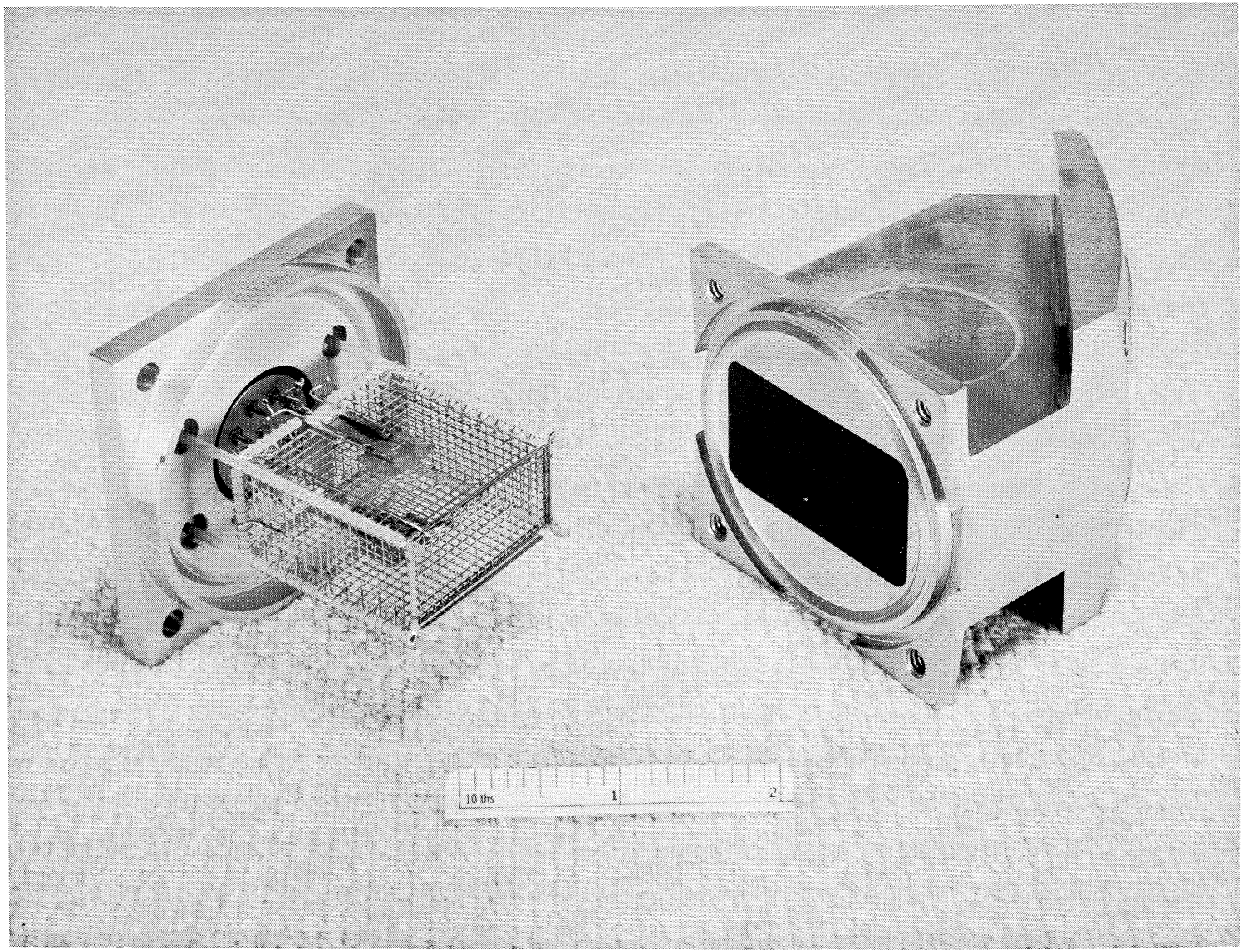

Fig. 5. Prototype omegatron assembly.

Fig. 6. Omegatron filament.

signs of deterioration. This level may be adequate for the first experimental models.

There are at least two possible methods of detecting the number of resonant ions in an omegatron. One is by collecting and measuring the outward spiraling ions as shown in Fig. 4. The other method, suggested by Sommer et al.,[12] is based on the fact that the kinetic energy of the ions increases as they spiral out [see Eq. (31)]. This energy is provided by the rf field; thus, by measuring the energy taken from the rf oscillator, one can determine the relative number of resonant ions. The latter method was tried in the laboratory without success, which was believed to be due primarily to the lack of ideal operating conditions. This approach requires a Pound-Knight type marginal oscillator, which is not a particularly difficult problem in the laboratory where constant adjustment can be made but poses a considerable problem in flight use. It was, therefore, decided to use the first method, that is, the collection of ions.

In the first experiment, this omegatron will not be used as a mass spectrometer, but rather as a partial pressure measuring sensor; keeping this in mind, an ion trajectory with 10 revolutions was selected. This will give a resolution of 17.6 at mass 28, which means that masses 29 and 27 could be separated. To decrease the influence of contact potentials, stray fields, etc., the rf field should be as large as possible, but once a permanent magnet is chosen, fixing the magnetic field strength the desired number of ion revolutions determines the magnitude of the electric field. Using Eq. (29), the required rf field strength for the above conditions is found to be 90 volts/meter. As the distance between the rf plates is 1.375-in., an rf voltage of approximately 6 volts peak to peak will be used. The total distance travelled by the ion in 10 revolutions is found from Eq. (33) to be 0.55 meters, which is small compared to the mean free path even at pressures as high as 10^{-5} mm Hg.

A typical spectrum obtained by this omegatron is shown in Fig. 7.

The merits and drawbacks of the omegatron as a mass spectrometer, based on the results of the theoretical and experimental investigations, may be summarized as follows:

Merits

(1) simple, rugged construction

(2) simple associated electronic circuitry

(3) small size

(4) low filament power requirement

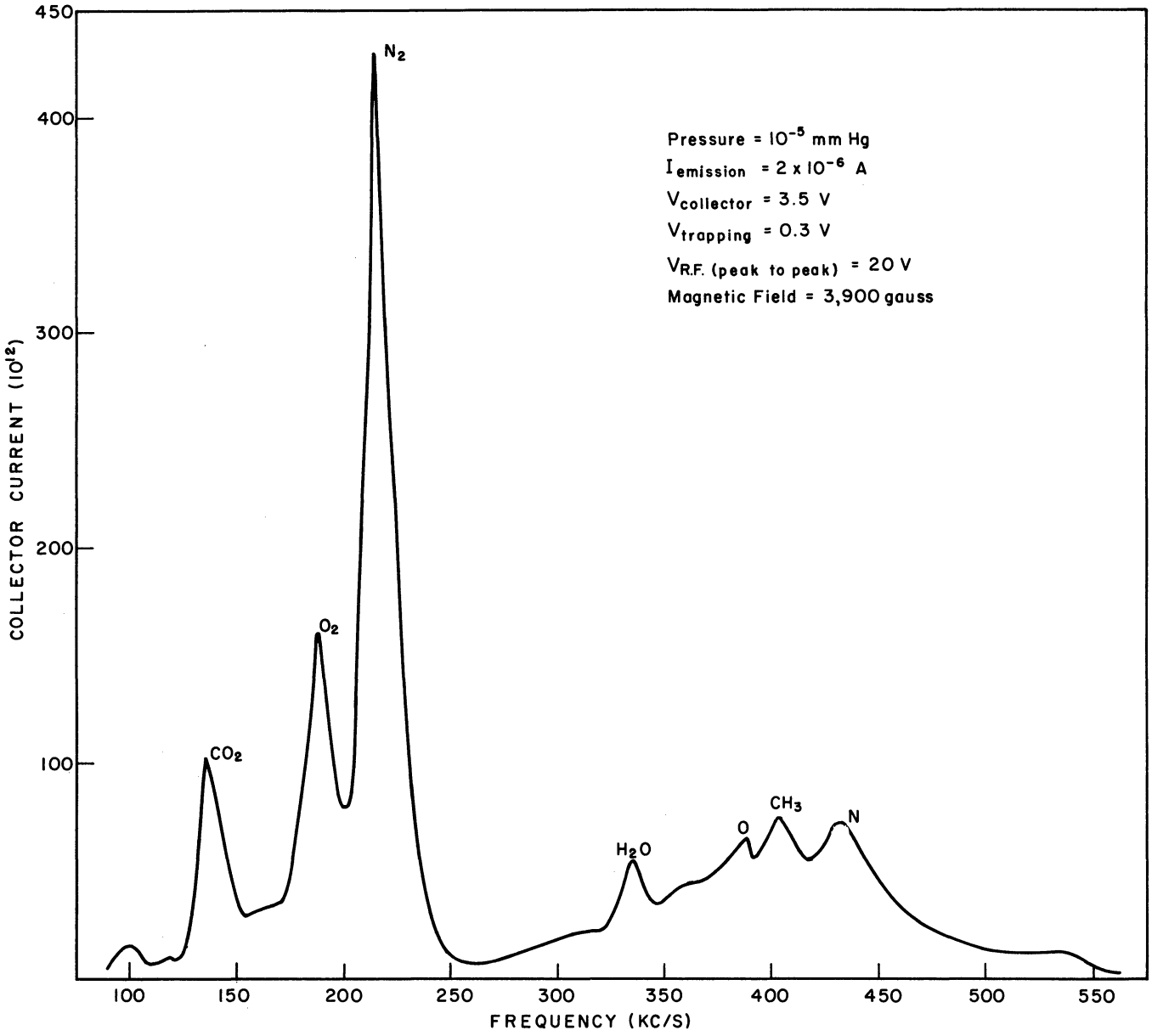

Fig. 7. Typical spectrum obtained by the omegatron.

(5) construction permits high conductance

(6) high sensitivity

(7) mass is a linear function of frequency

Drawbacks

(1) magnetic field is required, increasing the weight

(2) high resolution is generally accompanied by low sensitivity due to undesirable velocity components

(3) resolution is inversely proportional to the mass number

Based on the over-all experience gained with the omegatron, after considering its relative advantages and disadvantages, it can be said in summary that it is a simple and dependable device well suited for the proposed experiment.

The Westinghouse WX-4520 Bayard-Alpert ionization gage shown in Fig. 8 was selected for this experiment. These gages were provided by the Goddard Space Flight Center. It is a small, ruggedized gage especially designed for rocket and satellite experiments. It has three straight-line tungsten filaments, one used for normal operation, and two spares, but otherwise has a standard configuration. The gage was thoroughly calibrated on the vacuum system described in Section IV. Figures 9 and 10 show the variation of collector current versus collector voltage and grid voltage, respectively, for this gage. Figure 11 shows that the relationship between grid current and collector current is linear over the range of interest. Figures 12 and 13 illustrate the sensitivity curves for dry air and molecular nitrogen.

Due to the presence of large magnetic fields in the 13-in. sphere, it is necessary to shield the tube magnetically. To prevent the entrance of charged particles, which would cause erroneous pressure readings,[13] an ion trap is placed between the orifice and the gage itself. The mounting details of the complete assembly are shown in Fig. 14. As the drawing indicates, a backup vacuum seal is obtained with the aid of the magnetic shielding can, so that, should the glass envelope of the gage break, no gas can escape from the sphere to alter the ambient environment. The tube was not subjected to vibration, shock, and other mechanical tests in this laboratory as it has already proved itself in this respect in a number of rocket-borne experiments.

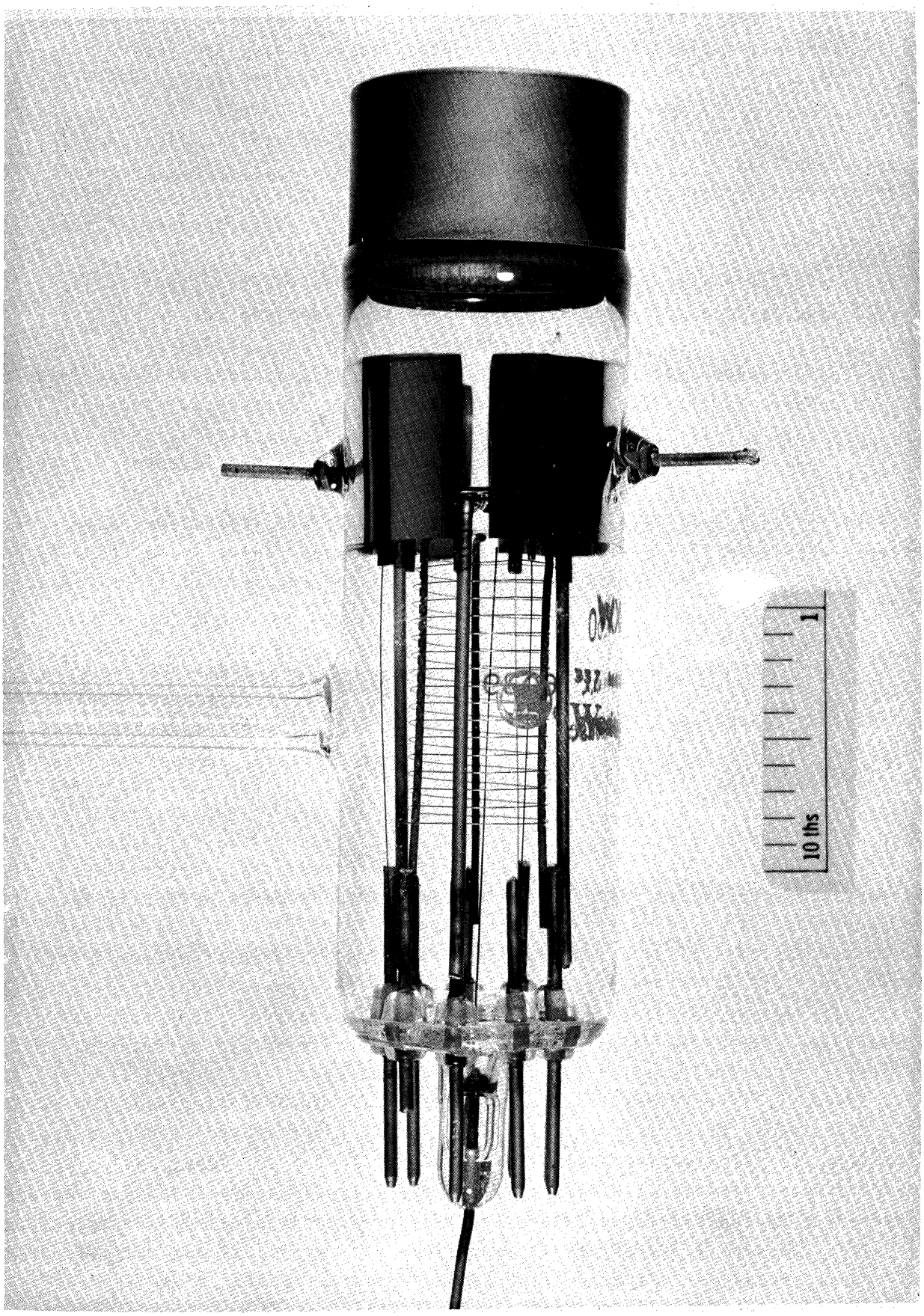

Fig. 8. Westinghouse WX-4520 Bayard-Alpert ionization gage.

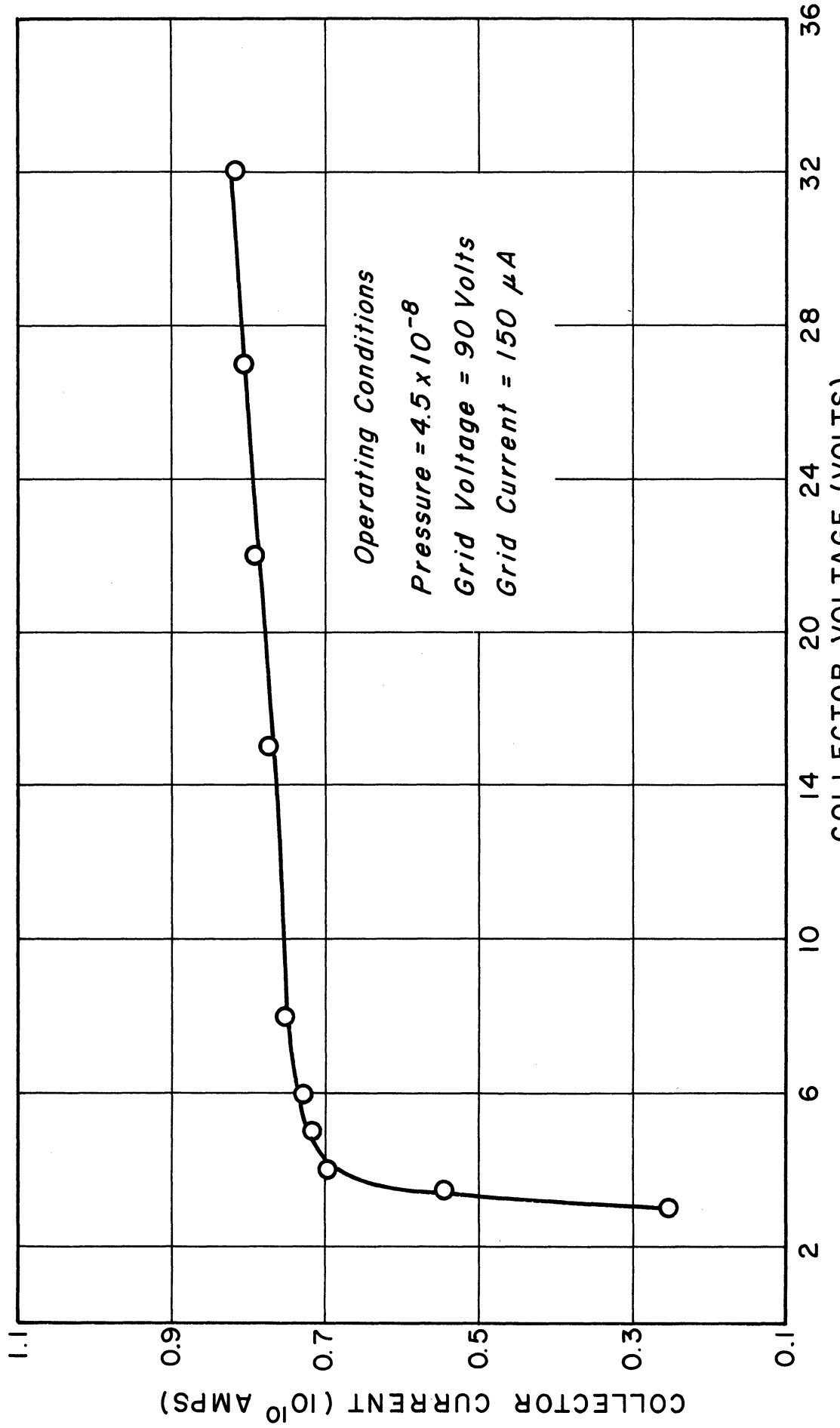

Fig. 9. Collector current versus collector voltage characteristics of a WX-4520 gage.

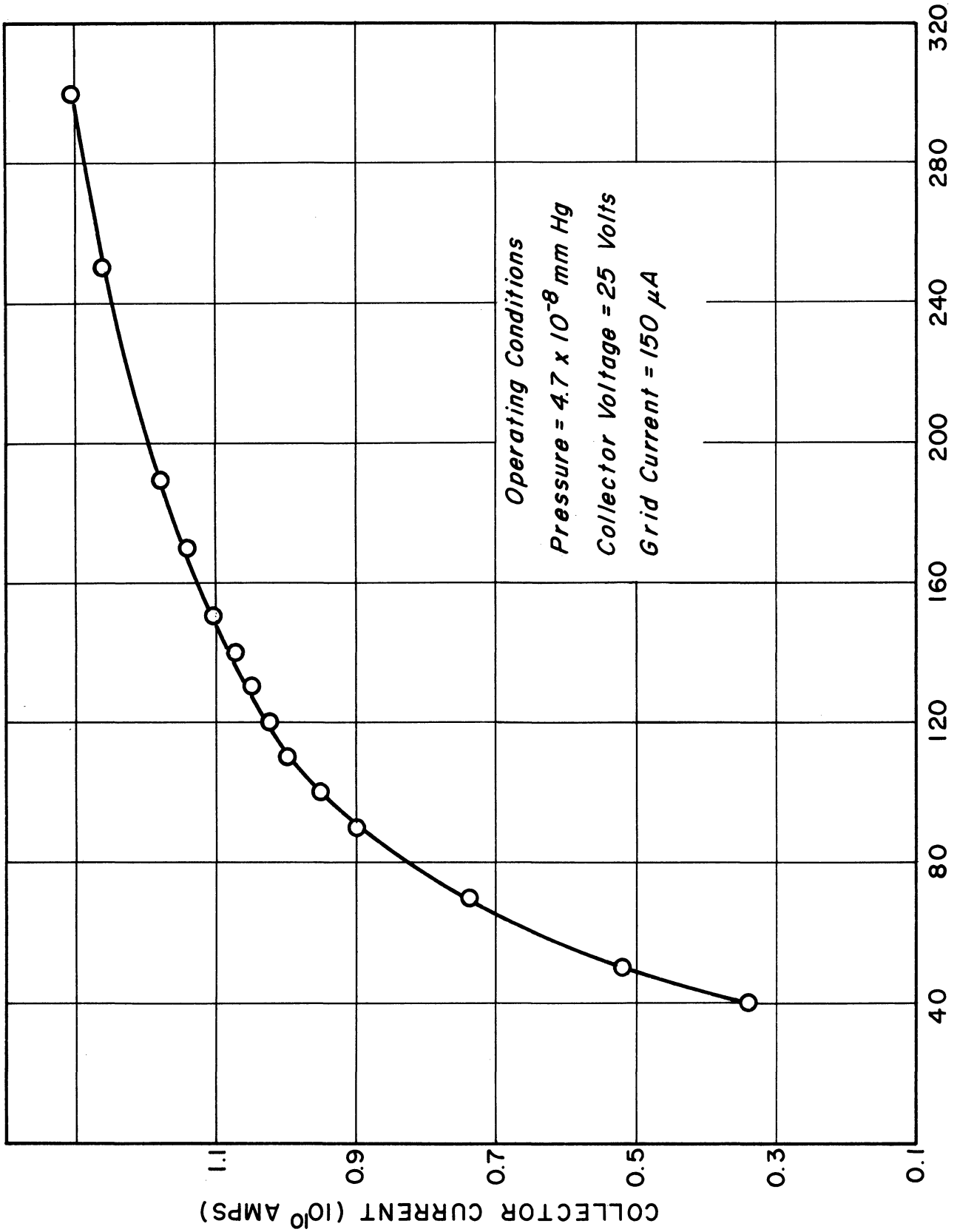

Fig. 10. Collector current versus grid voltage characteristics of a WX-4520 gage.

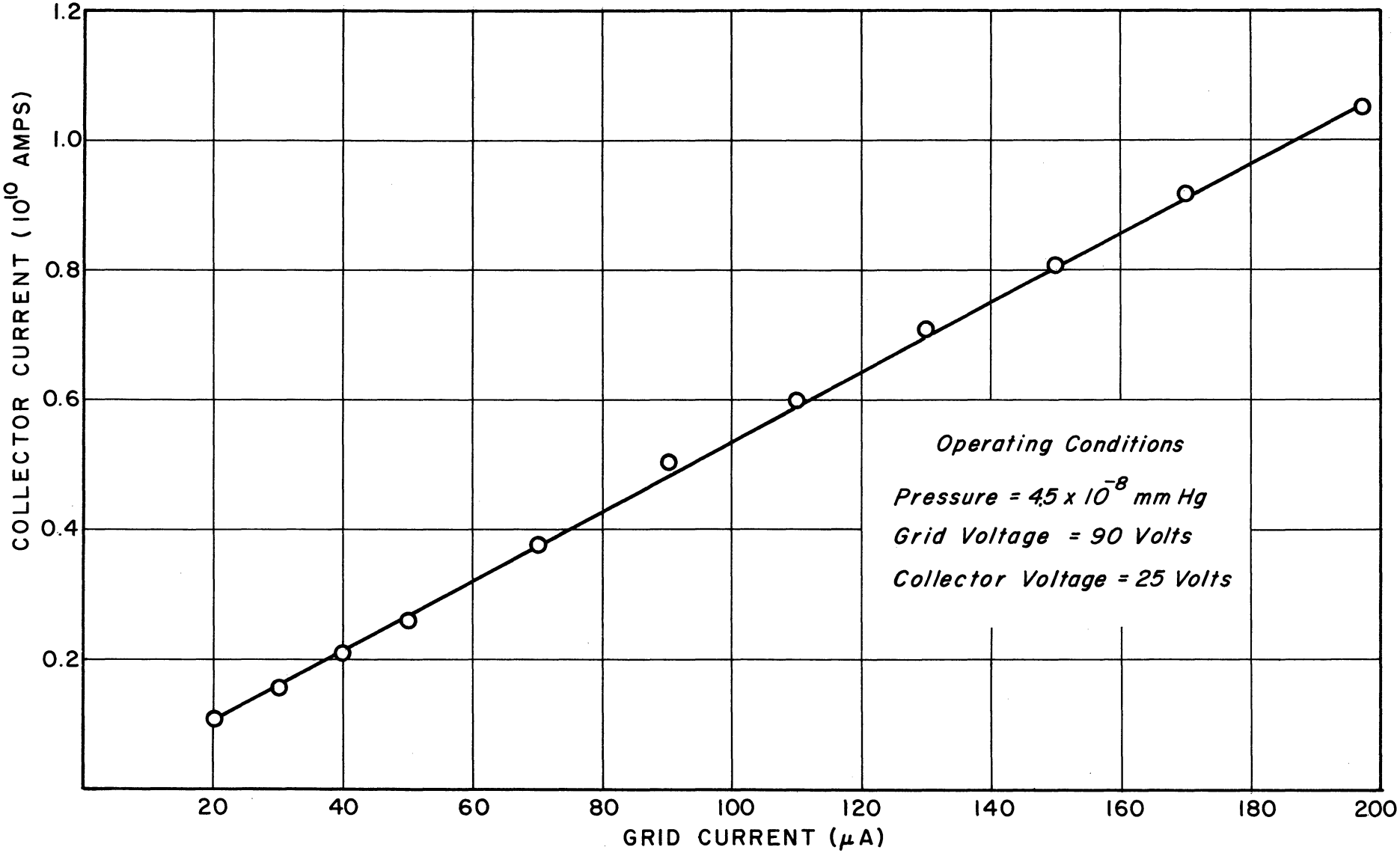

Fig. 11. Collector current versus grid current characteristics of a WX-4520 gage.

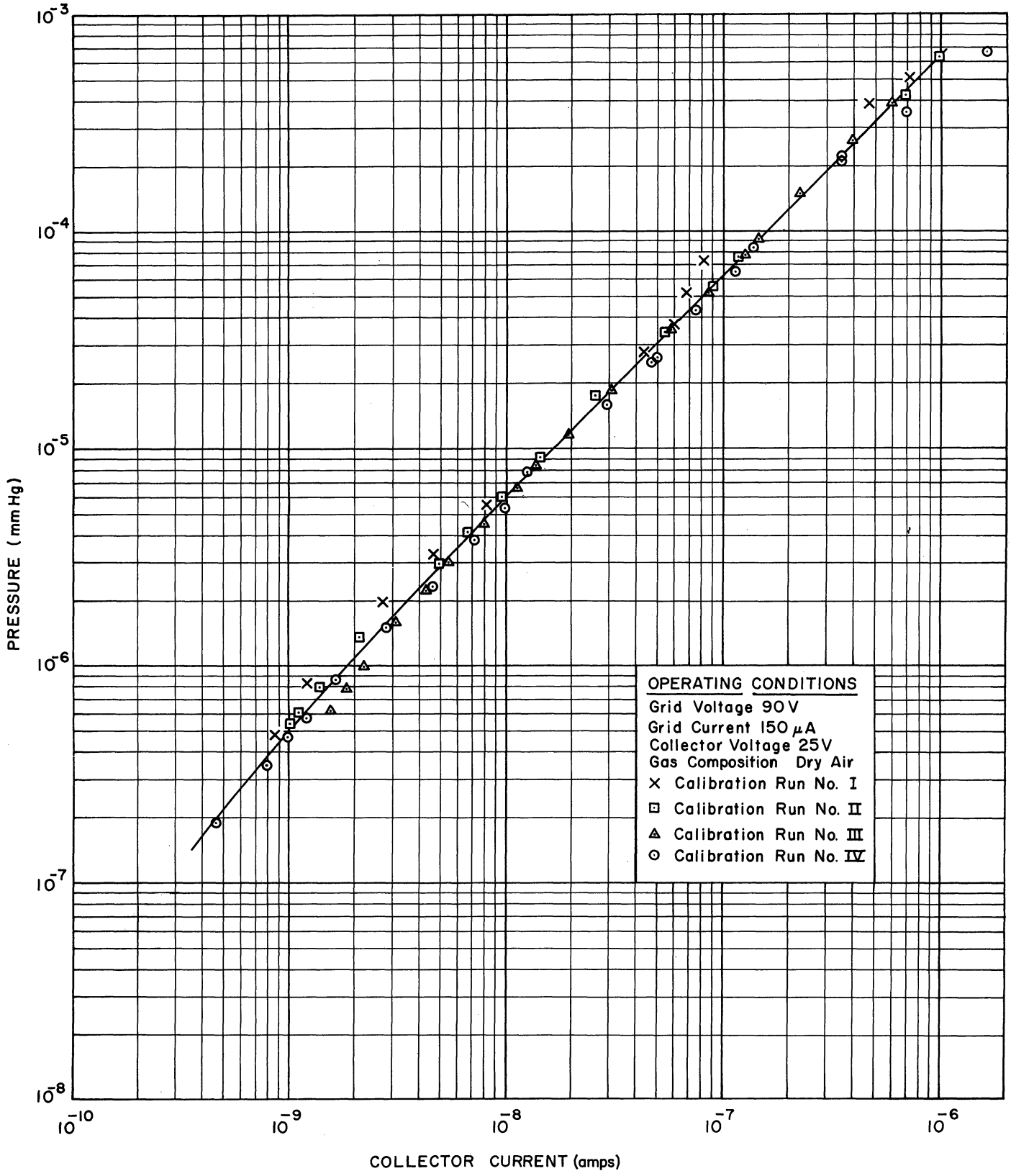

Fig. 12. Reference pressure versus collector current characteristics of a WX-4520 gage for dry air.

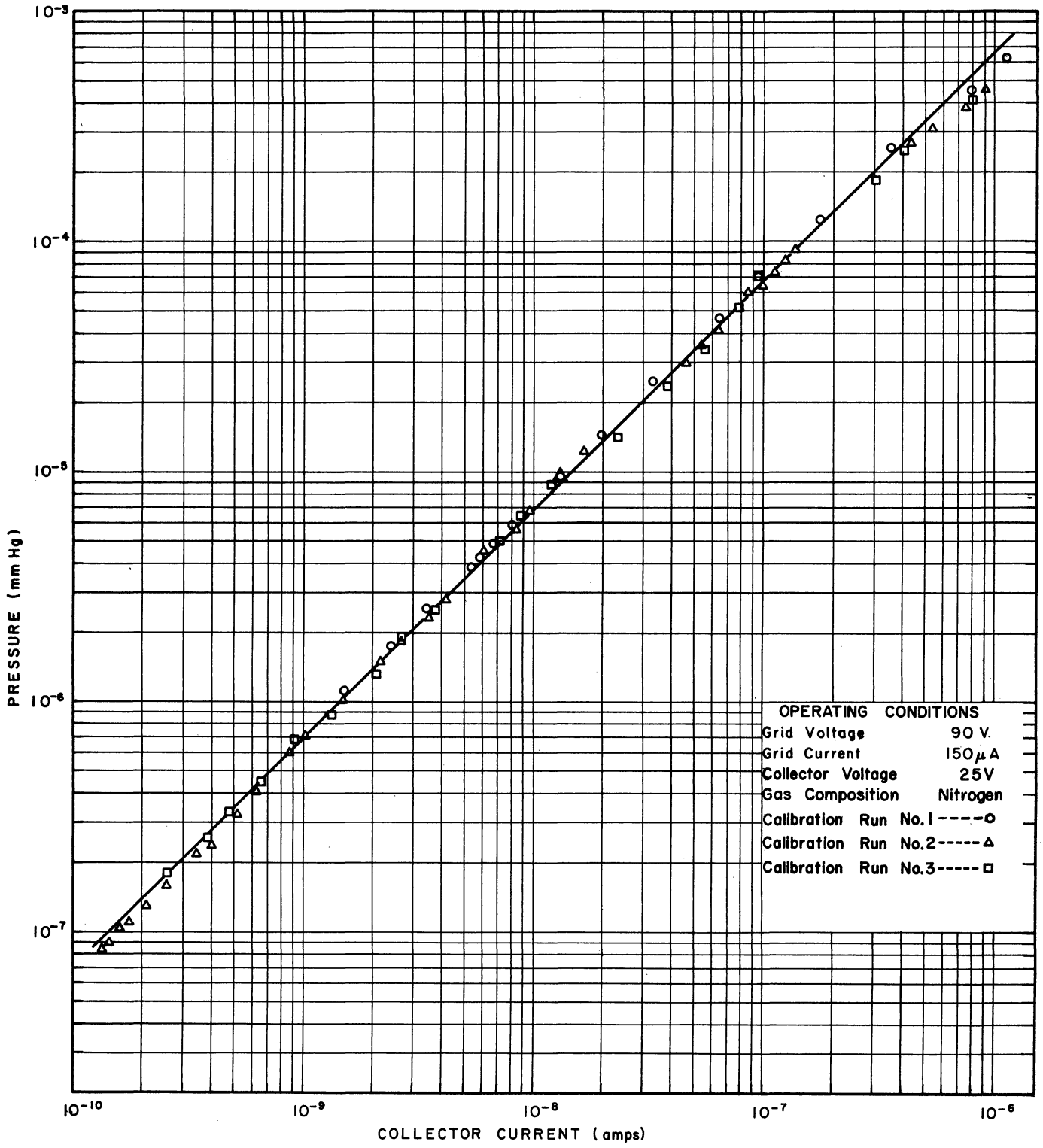

Fig. 13. Reference pressure versus collector current characteristics of a WX-4520 gage for nitrogen.

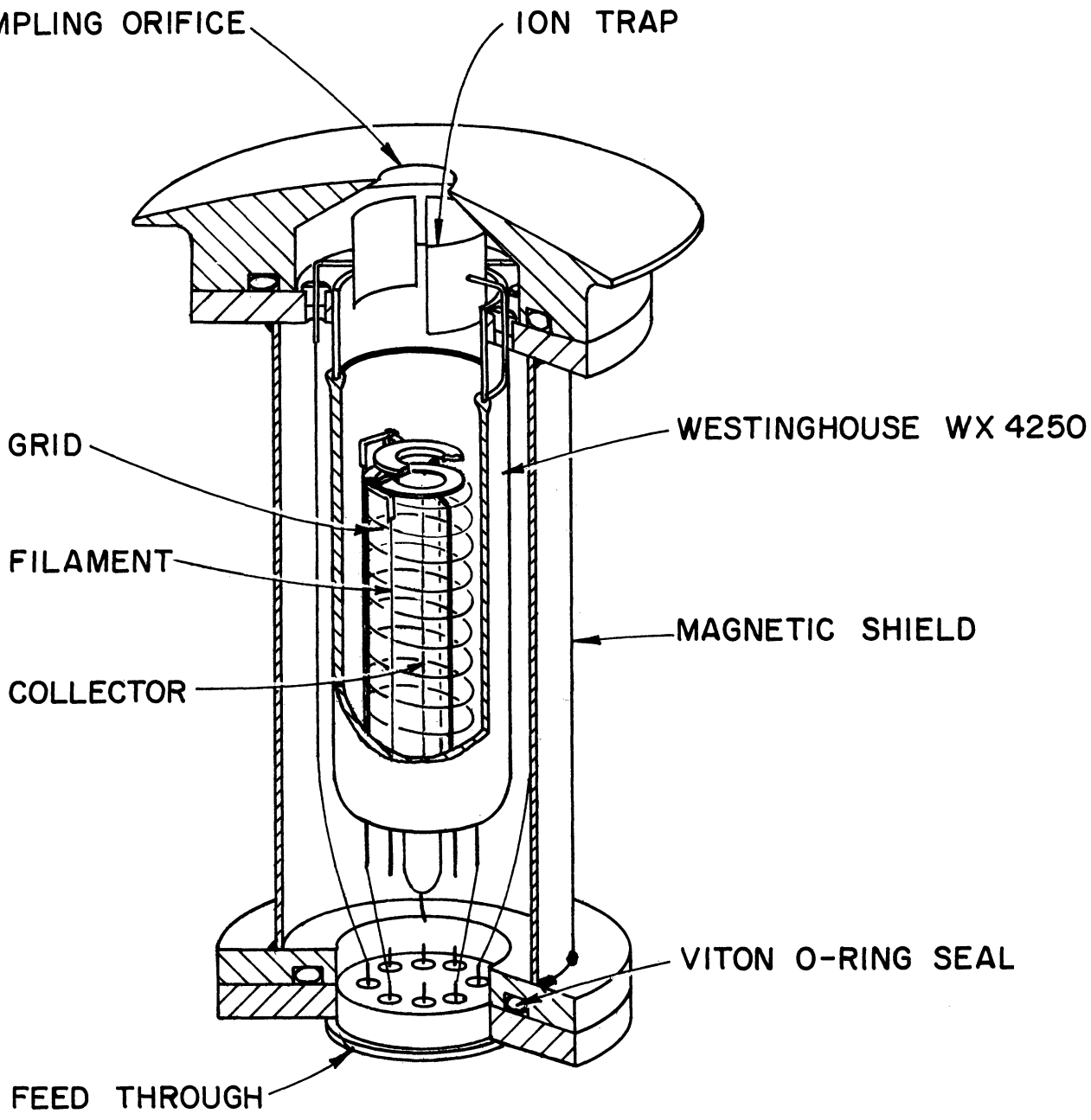

Fig. 14. The ionization gage assembly.

IV. VACUUM CALIBRATION SYSTEM

As indicated by Fig. 3, the sensors are to operate over an approximate pressure range of 10^{-4} to 10^{-8} mm Hg. A high-vacuum system was designed and built to permit a thorough calibration of the sensors in this range. Figure 15 and Figs. 16 and 17 respectively, show a block diagram and photographs of this vacuum system, which is of the type described by Alpert.[14] He has shown that at some pressure between 10^{-7} and 10^{-8} mm Hg the oil diffusion pump ceases to act as a sink and becomes a source of contamination; thus to obtain lower pressures, auxiliary means have to be used, which in this system is the pumping action of the ionization gages.

In this system to be described, the roughing pump is a Cenco HYVAC No. 7 having a pumping speed of 1.2 liters/second, and the oil diffusion pump is glass made by C.E.C. having a pumping speed of 25 liters/second. One-inch glass tubing is used to connect the diffusion pump to the bakable portion of the system, which consists of a high-conductance cold trap, three Granville Phillips Type C high-vacuum valves, and a number of ionization gages. This section is bakable to 450°C. In a typical operation the diffusion pump reduces the system pressure to about 10^{-7} mm Hg after an overnight bakeout. After this, the cold trap is filled with liquid nitrogen, the electrodes of the ionization gages are degassed by electron bombardment, and then valve No. 1 is closed and the ionization gages effect further pumping, achieveing an ultimate pressure of approximately 10^{-10} mm Hg in this sealed-off system.

To calibrate a given gage, it is mounted between two commercial Bayard-Alpert ionization gages. A pressure of about 10^{-9} to 10^{-10} mm Hg is first obtained and then through valves Nos. 2 and 3 a known gas is allowed to leak in slowly and the readings on all the gages noted. CEC GIC-013 gages are used as the comparison gages, these being calibrated by a McLeod gage. Clearly this is more of a secondary comparison than a calibration system, but for initial calibration it is considered to be sufficient. It is hoped that at a later date a more accurate calibration can be carried out on the flight gages at Goddard Space Flight Center.

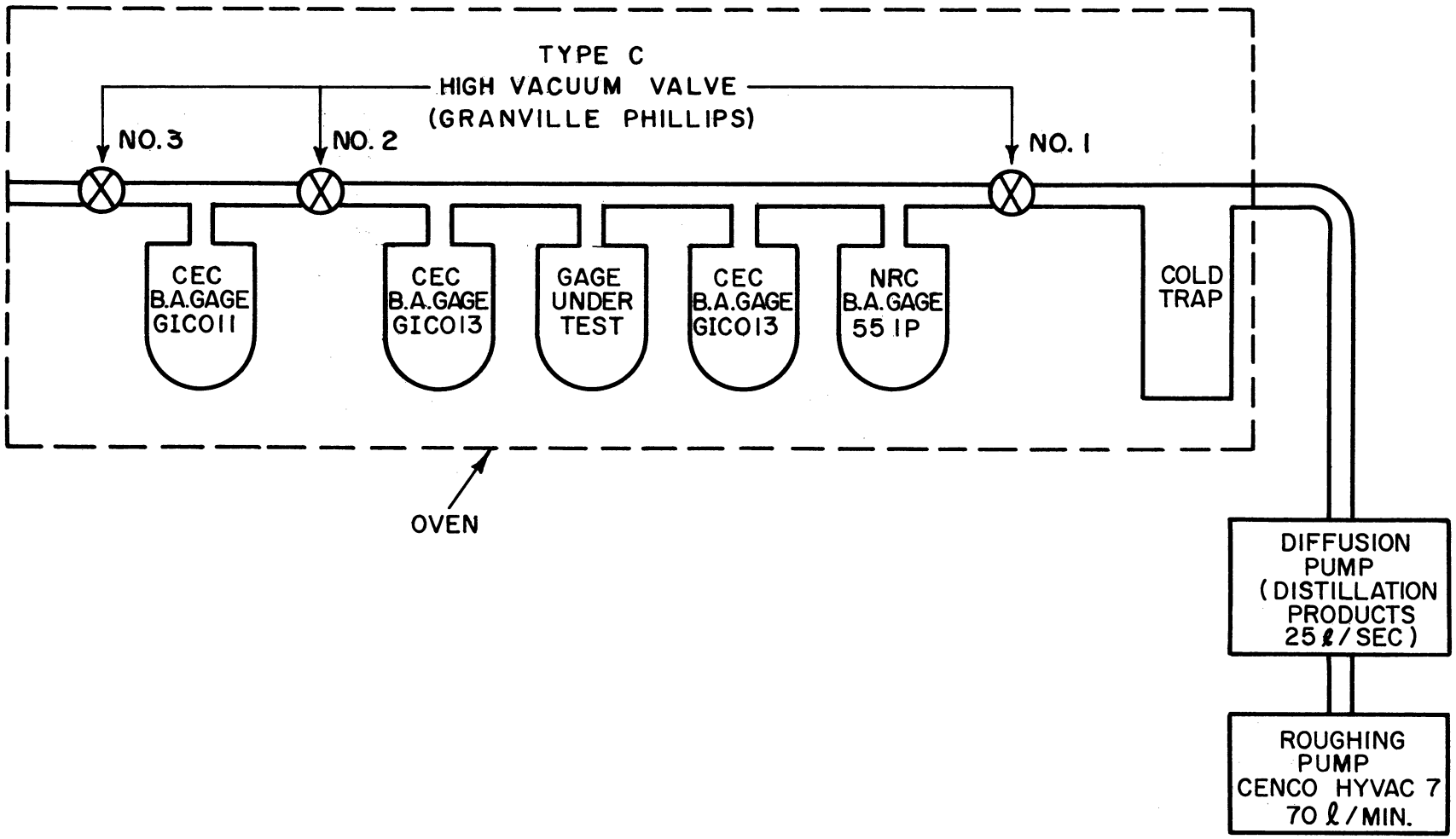

Fig. 15. Block diagram of the vacuum calibration system.

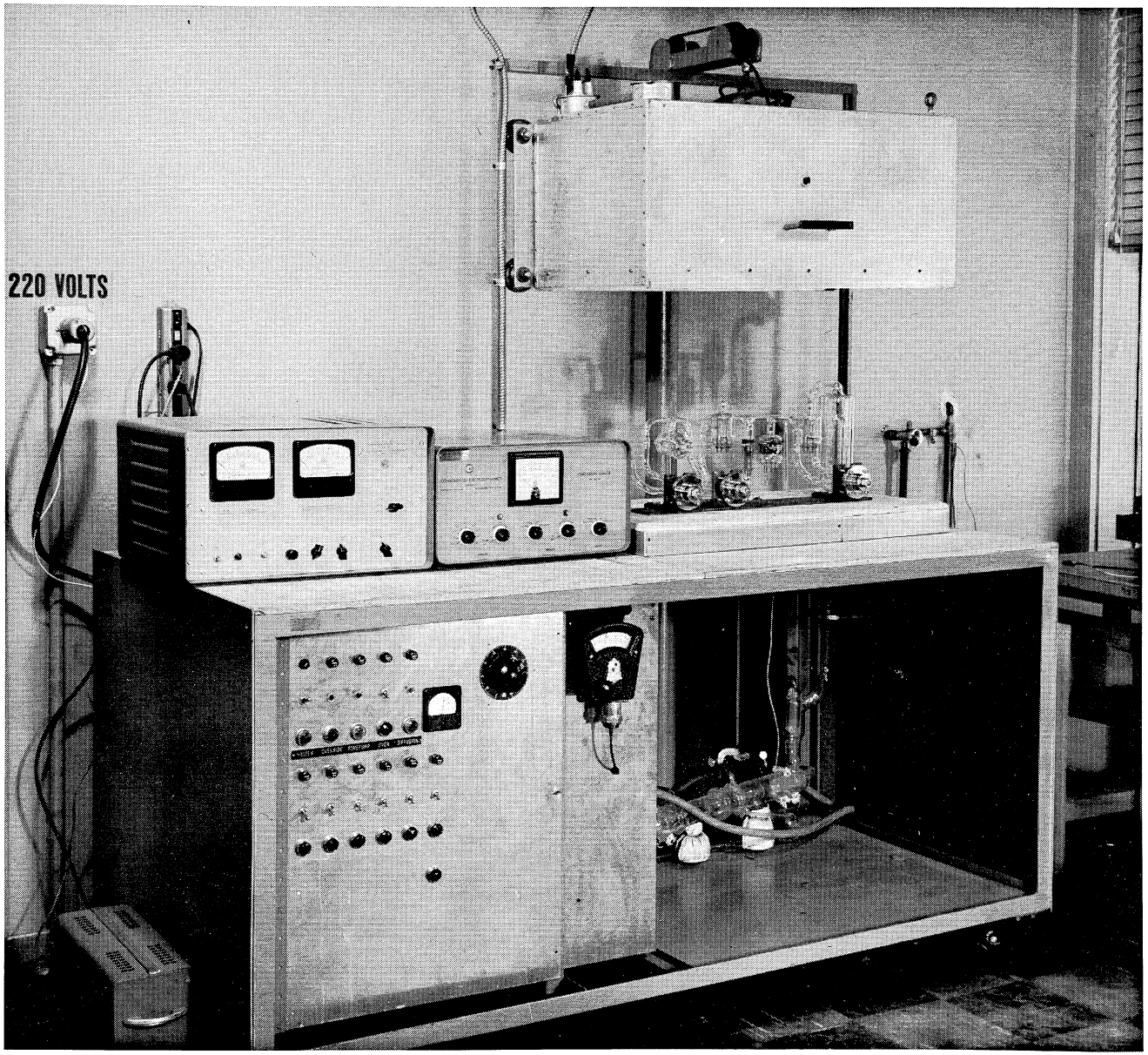

Fig. 16. Photograph of the complete vacuum system.

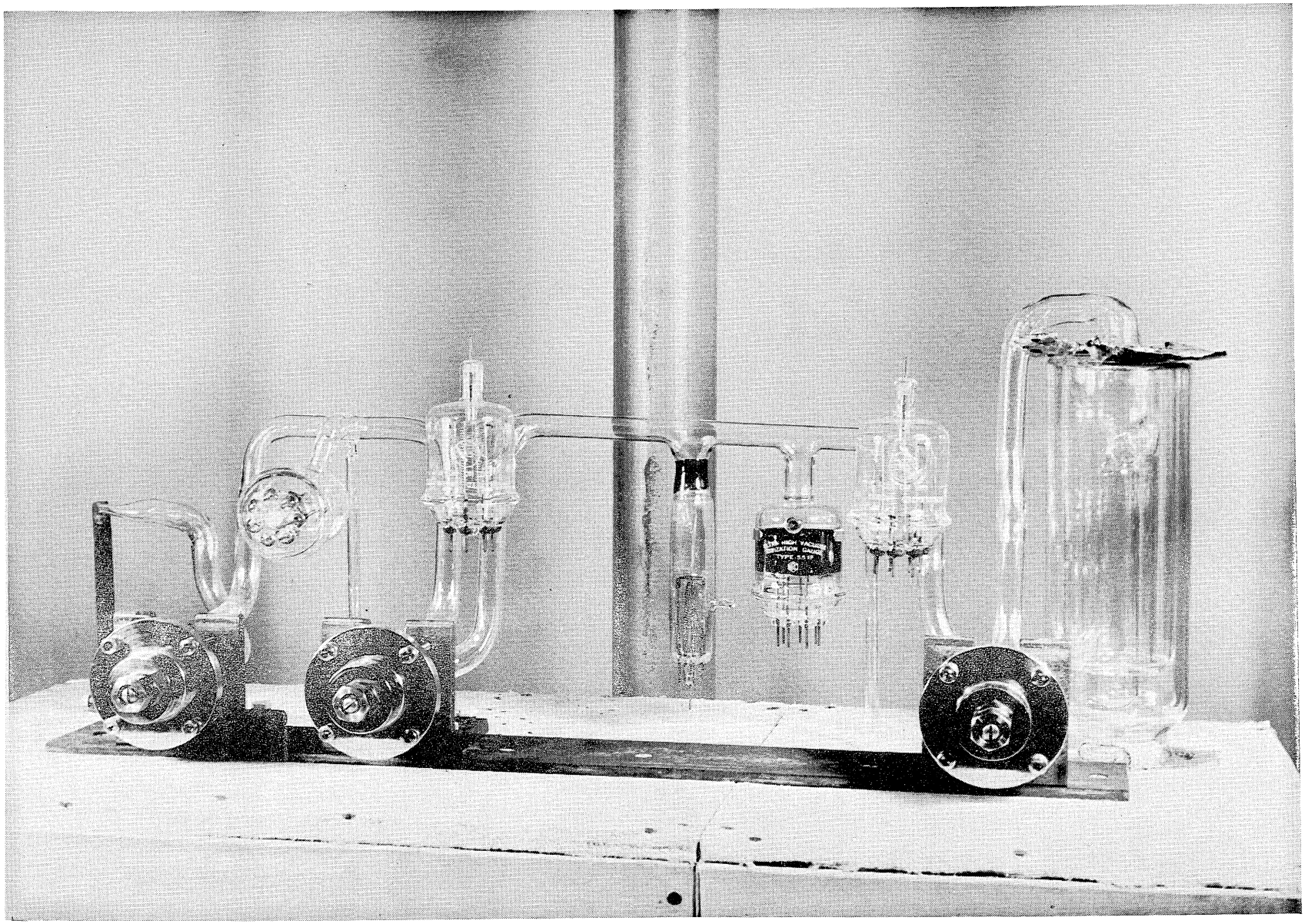

Fig. 17. The bakable portion of the vacuum system.

V. ELECTRONIC CIRCUITS

A. ELECTROMETER AMPLIFIER

The measurements of the resonant ions reaching the collector in the omegatron, as well as the measurement of collector current of the Bayard-Alpert gage requires a device which can convert these very small d-c currents to suitable voltage levels for telemetry. The smallest current expected is in the 10^{-12}-ampere range. A transistorized multirange electrometer amplifier (except for the electrometer) capable of measuring such low currents, which has been developed, built, and flown by this laboratory under another contract, will be used in this experiment. A general outline but no details of this amplifier will be given here as it has already been described in detail in another report.[15] The current to be measured is passed through a "hi-meg" resistor, and this voltage drop appears as a portion of the voltage in the feedback loop of a d-c amplifier for which β, the feedback factor, is unity. Thus a voltage change at the output of the amplifier is nearly equivalent in magnitude to the voltage change across the hi-meg resistor but opposite in sense. One can, in effect, consider the amplifier system as an impedance-matching device. The transfer function of this feedback amplifier is given by

$$K = \frac{E_{\text{output}}}{I_{\text{input}}} = R_f = \frac{A}{1 - A\beta}$$

where

A = open-loop gain of amplifier
R_f = feedback resistor

The open-loop gain is between one and two thousand; thus the closed loop gain is very close to one, and is practically insensitive to open-loop-gain variations. The currents to be measured in this experiment are expected to vary over five decades so the amplifier should have a number of different current ranges. This is done by changing the hi-meg resistors by means of a fully automatic range-switching circuit incorporated into the system. The circuit diagram of the complete system is given in Fig. 18, and for a detailed description one may refer to the report mentioned earlier. Figure 19 is a photograph of this unit.

B. EMISSION REGULATORS

The filaments of both the omegatron and the ionization gage must maintain a constant emission over a wide range of ambient conditions, and to achieve

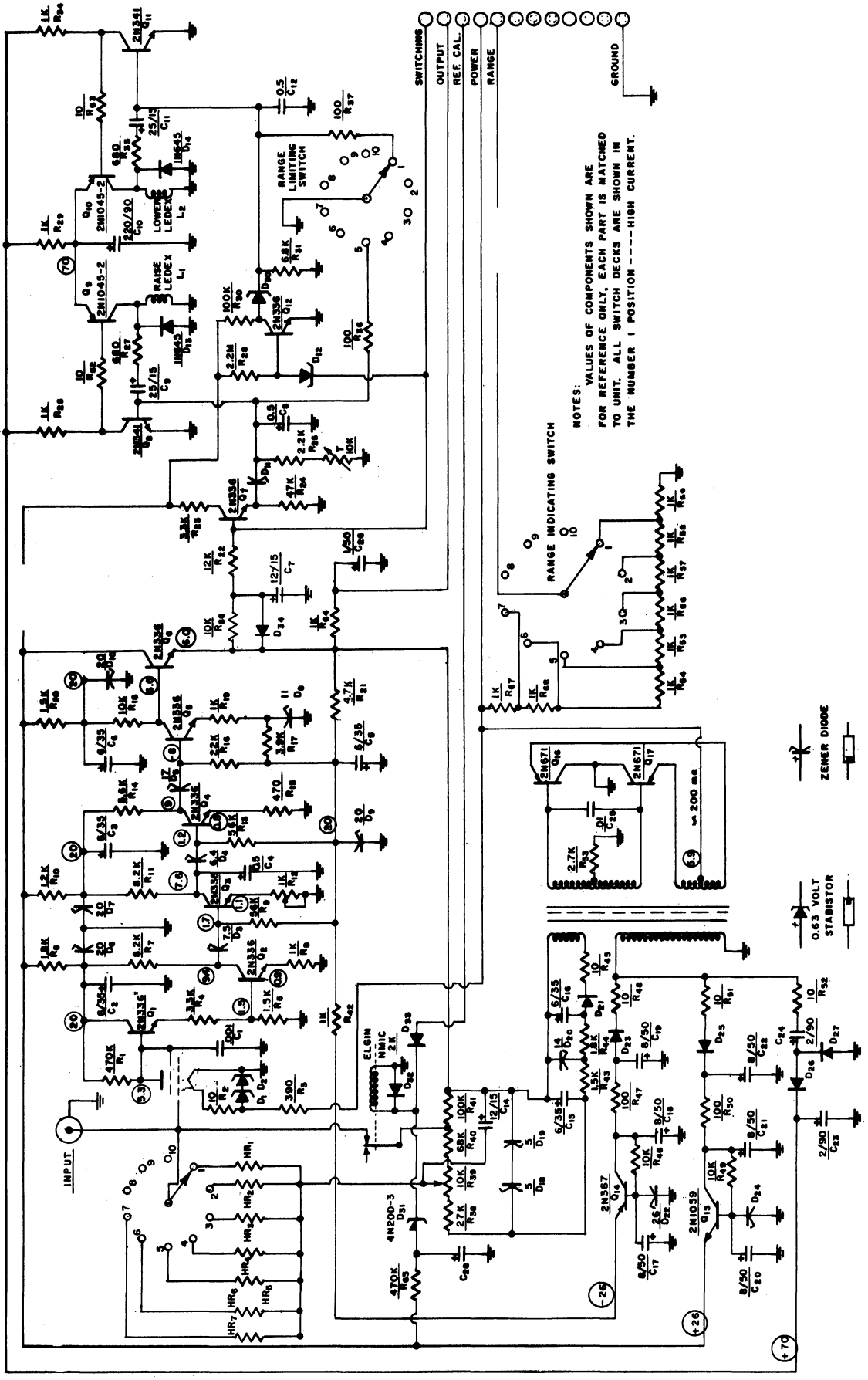

Fig. 18. Circuit diagram of the electrometer amplifier.

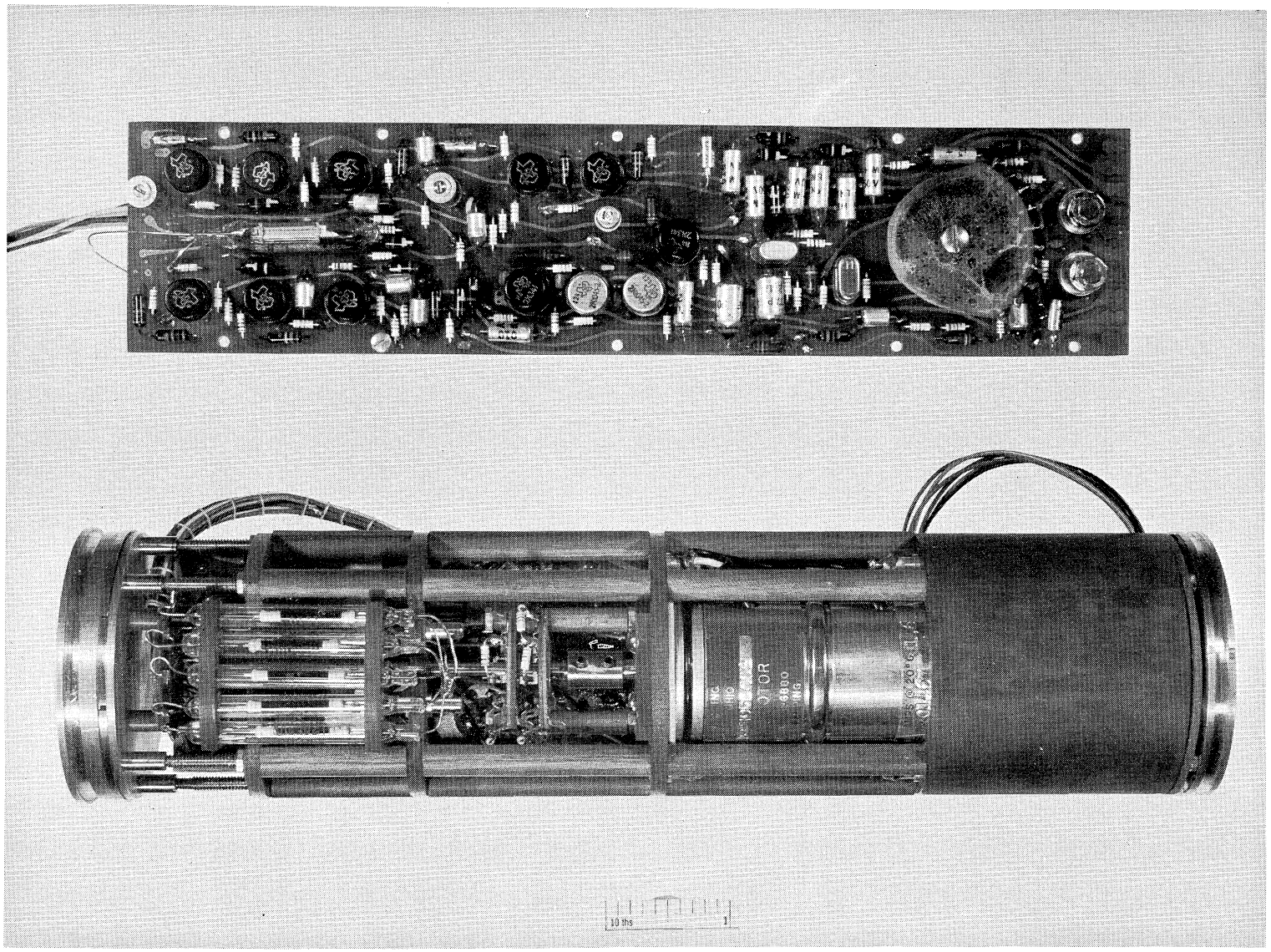

Fig. 19. Top and bottom view of the electrometer amplifier.

this a filament regulator is necessary. Figures 20 and 21 show the series-type regulator developed for the ionization gage and the omegatron, respectively. The two circuits are basically identical; the only difference is in the input stage, as the base current of transistor Q_5 should be at least 10 μA to minimize drifts. The ionization gage operates with an emission current of approximately 150 μA, so the base current is a small fraction of this current, and is set by potentiometer P_1. On the other hand, the omegatron which operates with a beam current of only a few microamperes, needs the biasing arrangement, consisting of the zener diode D_1 and potentiometer P_1, to get this required current. The emitter coupled amplifiers Q_4 and Q_5 are followed by a conventional common emitter stage Q_3, the output of which is connected to the base of Q_2. Transistors Q_1 and Q_2 are connected as double emitter followers, and they act as the regulating element.

Temperature tests on the ionization gage and omegatron regulators showed that when operating them at 150 μA and 5 μA, respectively, the variation in emission current was less than 1% up to 60°C. The variation in the emission current is less than 1% when supply voltage E_1 changes from 26V to 32V, and less than 1% when supply voltage E_2 changes from 3.5 to 8V.

A simple switching circuit is incorporated into the ionization gage regulator which will switch from one filament to another in case a filament breaks during flight. This circuit is shown in Fig. 22. In a series regulator when the load is removed, the output voltage will be approximately the same as the supply voltage. The switching circuit uses this increase in the output voltage to sense the filament burnout. This voltage increase causes the current in transistor Q_1 to increase sufficiently to energize the microminiature GE "Unimite" type relay in the collector circuit. A fuse is placed in parallel with the relay coil to provide a short time delay so as to avoid the possibility of a switchover being caused by some random pulse. This switchover circuit was thoroughly tested and was found to operate satisfactorily in a pressure range of 10^{-8} to 10^{-4} mm Hg, and at temperatures up to 60°C.

In these series-type regulators a large fraction of the power from the battery is lost in the series transistor, thus increasing the ampere-hour capacity requirement of the battery and also presenting a secondary problem in heat dissipation. For this reason a switching-type filament regulator (Fig. 23) for the thermionic gage was also developed to be used when maximum efficiency is required. This regulator is basically an asymmetric free-running multivibrator with controllable on-off periods. The thermal time constant of the filament is large (in the order of a second) so a frequency of about 1000 c/s was found to be more than sufficient to avoid fluctuations in the emission and at the same time not too high to decrease the efficiency appreciably. Transistors Q_4, Q_5, and Q_6 make up the emitter coupled multivibrator. The filament of the device to be regulated is used as the common emitter resistor. Transistors Q_5 and Q_6 are connected as double emitter followers. To obtain maximum battery economy the power supply is made up of the following: four high-current-

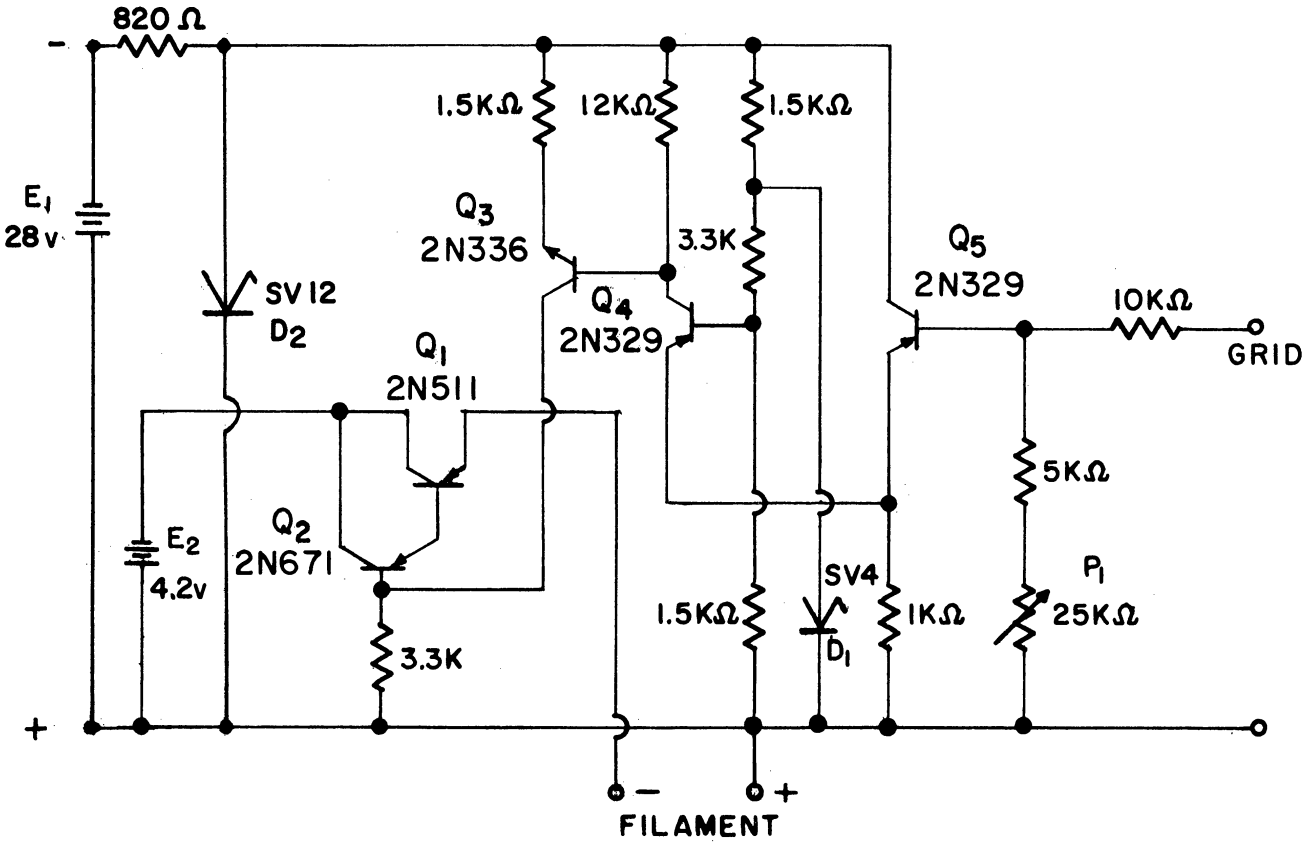

Fig. 20. Circuit diagram of the ionization gage filament regulator.

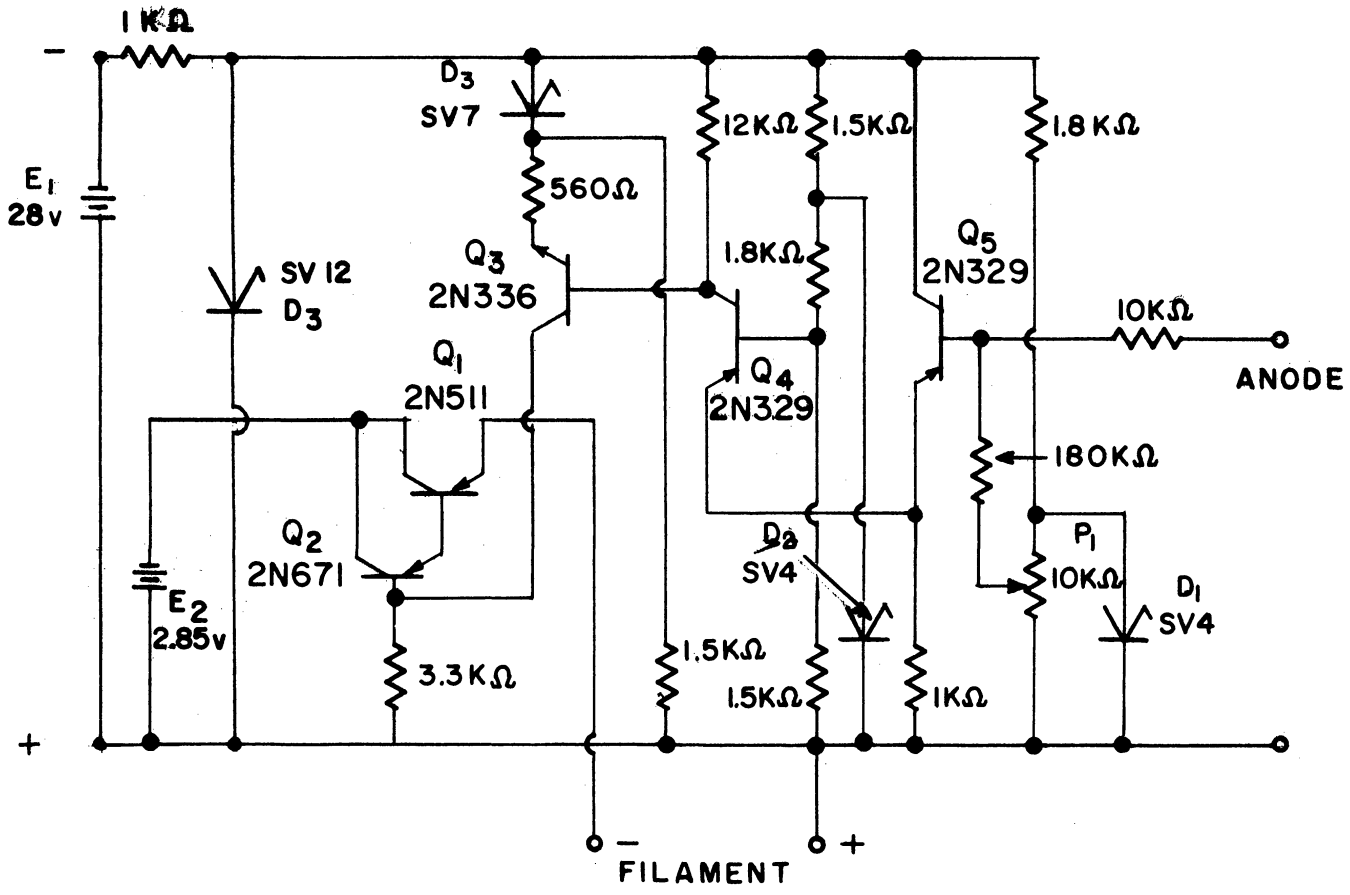

Fig. 21. Circuit diagram of the omegatron filament regulator.

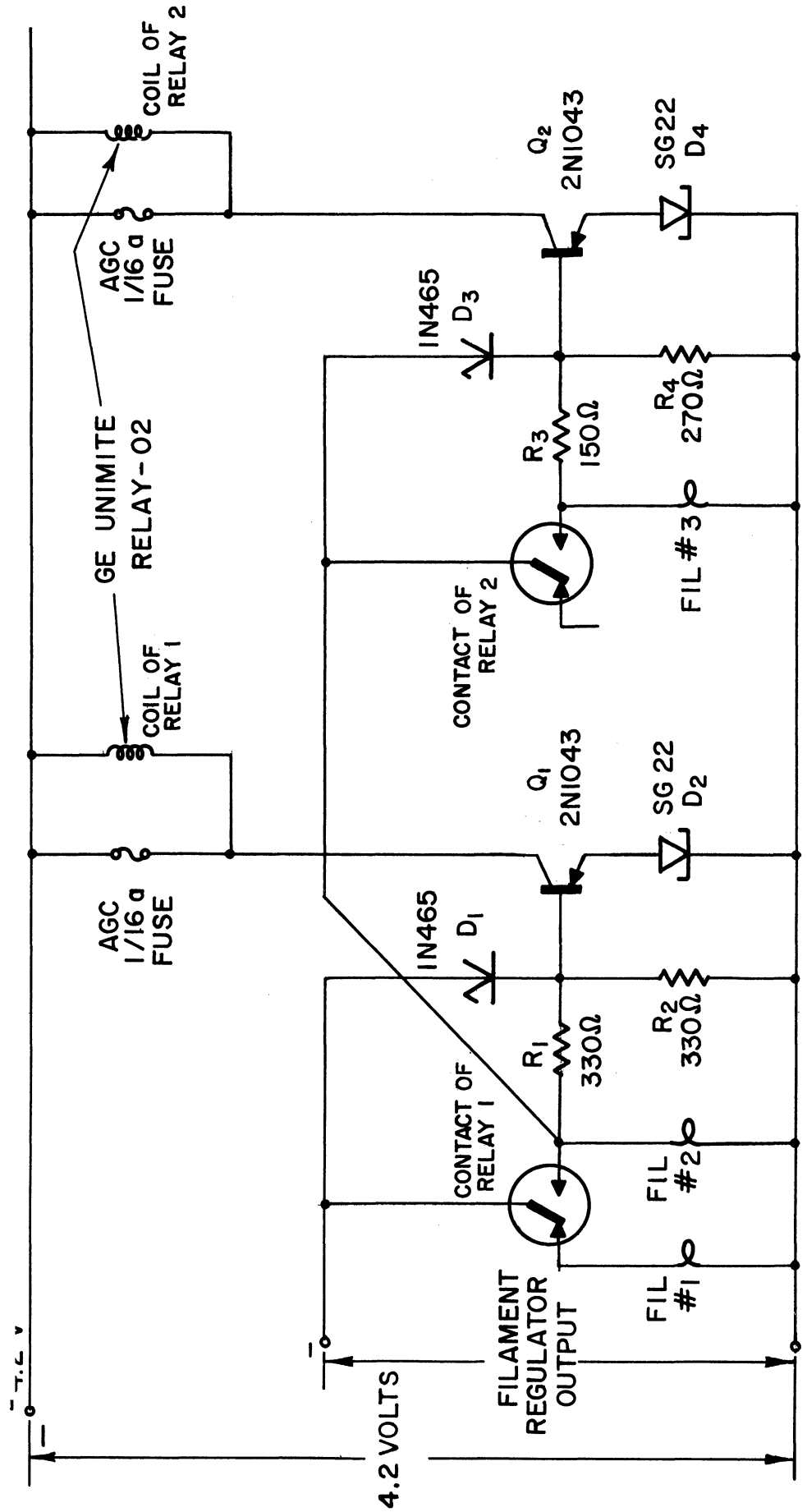

Fig. 22. Circuit diagram of filament switch over circuit.

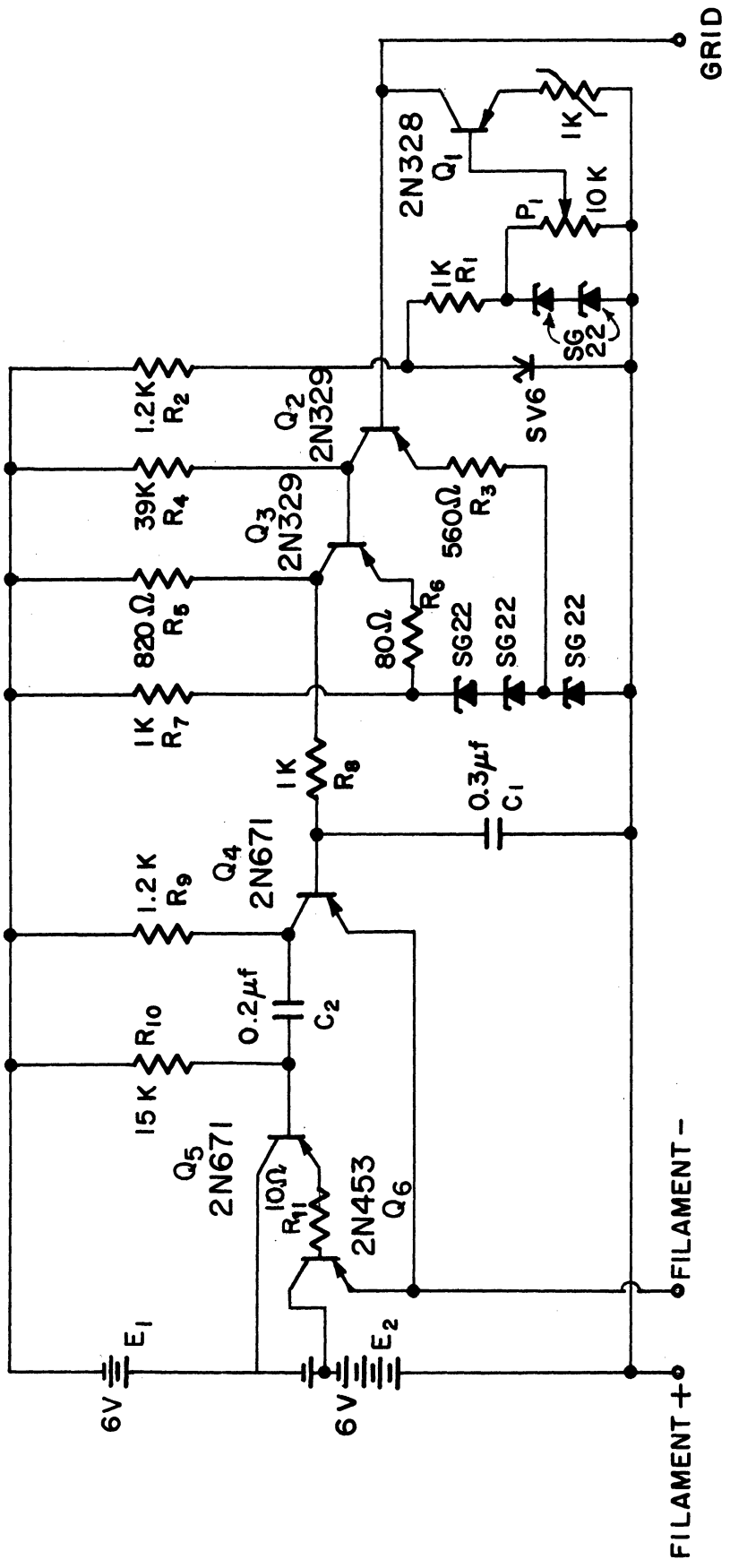

Fig. 23. Circuit diagram of switching-type filament regulator.

capacity Silver Cells in series giving 6.0 volts, providing the filament power, and a 6-volt mercury battery connected in series with it to give a total of 12.0 volts to supply the lower current requirement of the rest of the circuit. The $R_{10}C_2$ combination sets the fixed "off" time of the Q_5 and Q_6 section, whereas the variable "on time" is determined by the R_8C_1 combination and the potential at the collector of Q_3. This potential is set by Q_3 and Q_2 which are connected as conventional common emitter amplifiers. To get maximum sensitivity, the base current of Q_2 is the algebraic difference between the current from the constant current supply and the emission current of the device to be regulated. Potentiometer P_1 permits adjustment in the emission level of the filament.

Extensive temperature tests showed that the only component requiring temperature compensation is transistor Q_1 of the reference supply. It has been found[16] that temperature drifts in silicon transistors, properly biased and operating at temperatures below 80°C, cause changes in the base to emitter voltage drop V_{be}. These changes are a linear function of temperature, so they can be compensated by positive temperature coefficient resistors. Compensation was effected in our circuit by placing a Texas Instrument 1 KΩ Sensitor in series with the emitter of Q_1. With this compensation, the variation in the emission current was less that 1% up to temperatures of 60°C. It was also established that emission current stays constant, to within 1% when E_1 changes from 2.5 to 7.5 volts and within 4% when filament supply E_2 changes from 5.5 to 7.5 volts. The over-all efficiency of the regulator was found to be 90-95% depending on the operating conditions.

C. VOLTAGE SUPPLY

The 400-cps square wave voltage (available from the d-c to d-c convertor of the electrometer amplifier system) is used after rectification to provide the high voltages necessary to operate the ionization gages and the omegatron. Figure 24 shows the circuit diagram of such a rectifier which consists of two

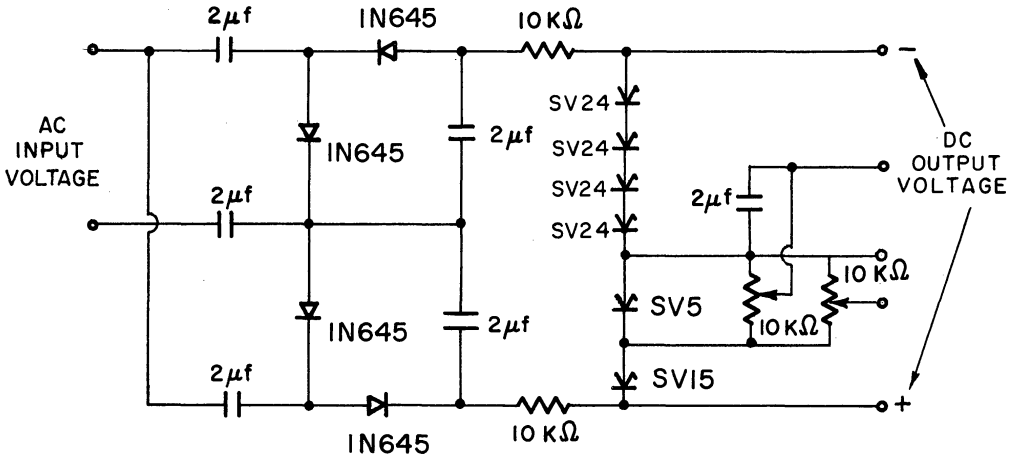

Fig. 24. Circuit diagram of high-voltage supply.

voltage doublers in series, having a floating center point. Zener diodes are used to provide a regulated output voltage of approximately 110 volts. The potentiometers permit the necessary adjustments for optimizing the operating conditions for the omegatron.

D. RF OSCILLATOR

In the first experiment the omegatron will be "tuned to N_2"; hence a stable, fixed frequency oscillator is required. The oscillator circuit shown in Fig. 25 was designed for this purpose. It consists of two stages, a self-excited oscillator and a buffer stage.

The resonant frequency of the oscillator is determined by L_1, C_5, and C_6. The variable inductor permits a small frequency adjustment of about 5%. The temperature coefficients of C_1 and C_2 were chosen to be slightly positive to compensate the temperature coefficient of L_1. This gives a frequency stability of 0.06% over a temperature range of 0-60°C. Potentiometer P_1 in the emitter of Q_2 permits adjustment of the output voltage from 3 to 12 volts peak to peak. The shunt resistor R_9 is placed parallel to the input of the buffer stage to keep the load on the oscillator relatively constant. The output voltage is kept constant well within 1% over a temperature range of 0-60°C by including a sensistor in the load circuit of Q_2. The balanced output required for the omegatron is obtained by using a transformer. The d-c voltage developed across R_{16} is used to monitor the output voltage. With the power supply voltage varying between 24 and 32 volts, the output voltage variation was well below 1% and no frequency change was detectable.

E. TELEMETRY

The Vector TRPT-250-R, 1/3-watt, all-transistor FM-FM telemetry transmitter has been chosen as suitable for this experiment, taking into consideration such factors as size, availability, and r-f power requirements. Vector TR30 S.C.O.'s, which were especially designed to operate with this transmitter, will be used.

After numerous tests it was decided to use two quarter-wavelength whip antennas mounted 180° apart on the sphere, parallel to the axis of rotation. The measured radiation pattern of this configuration, shown in Fig. 26, is very similar to that of a dipole. Experience from previous flights indicates that, with a 1/3-watt transmitter, there should not be any signal strength problem.

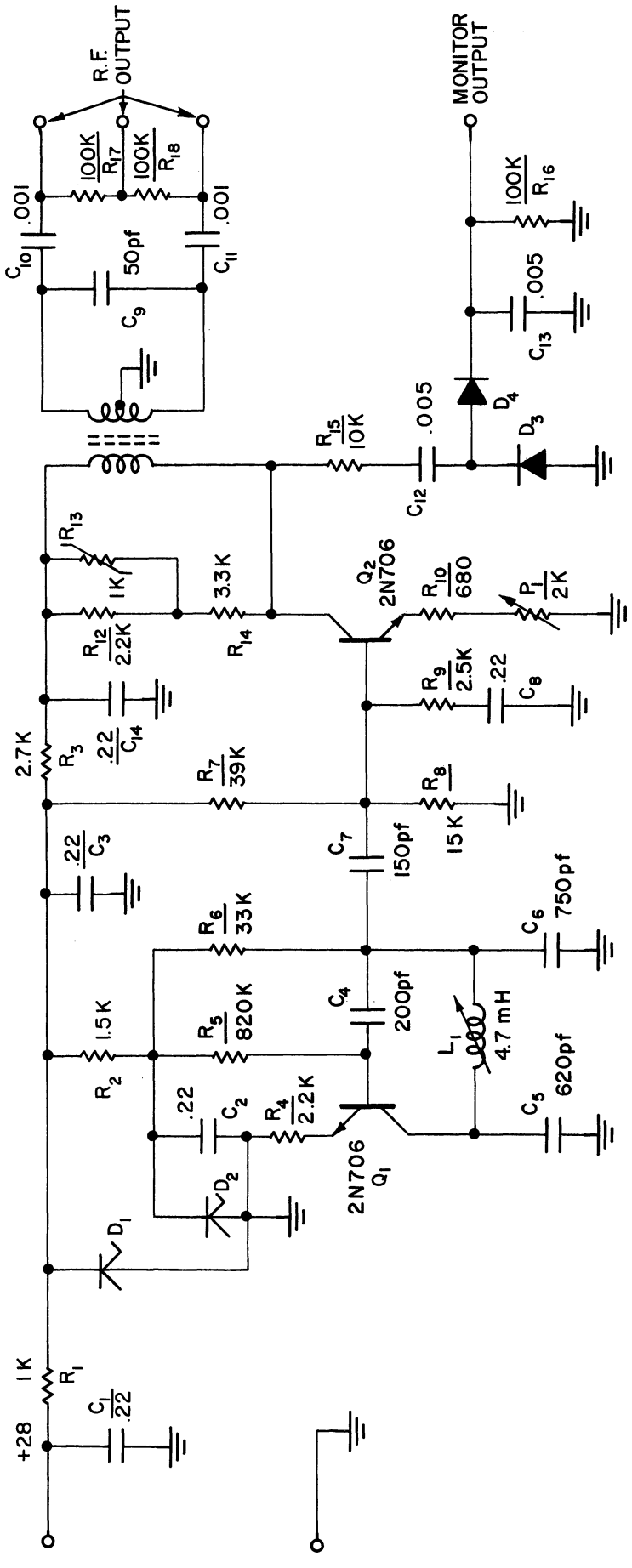

Fig. 25. Circuit diagram of the omegatron rf oscillator.

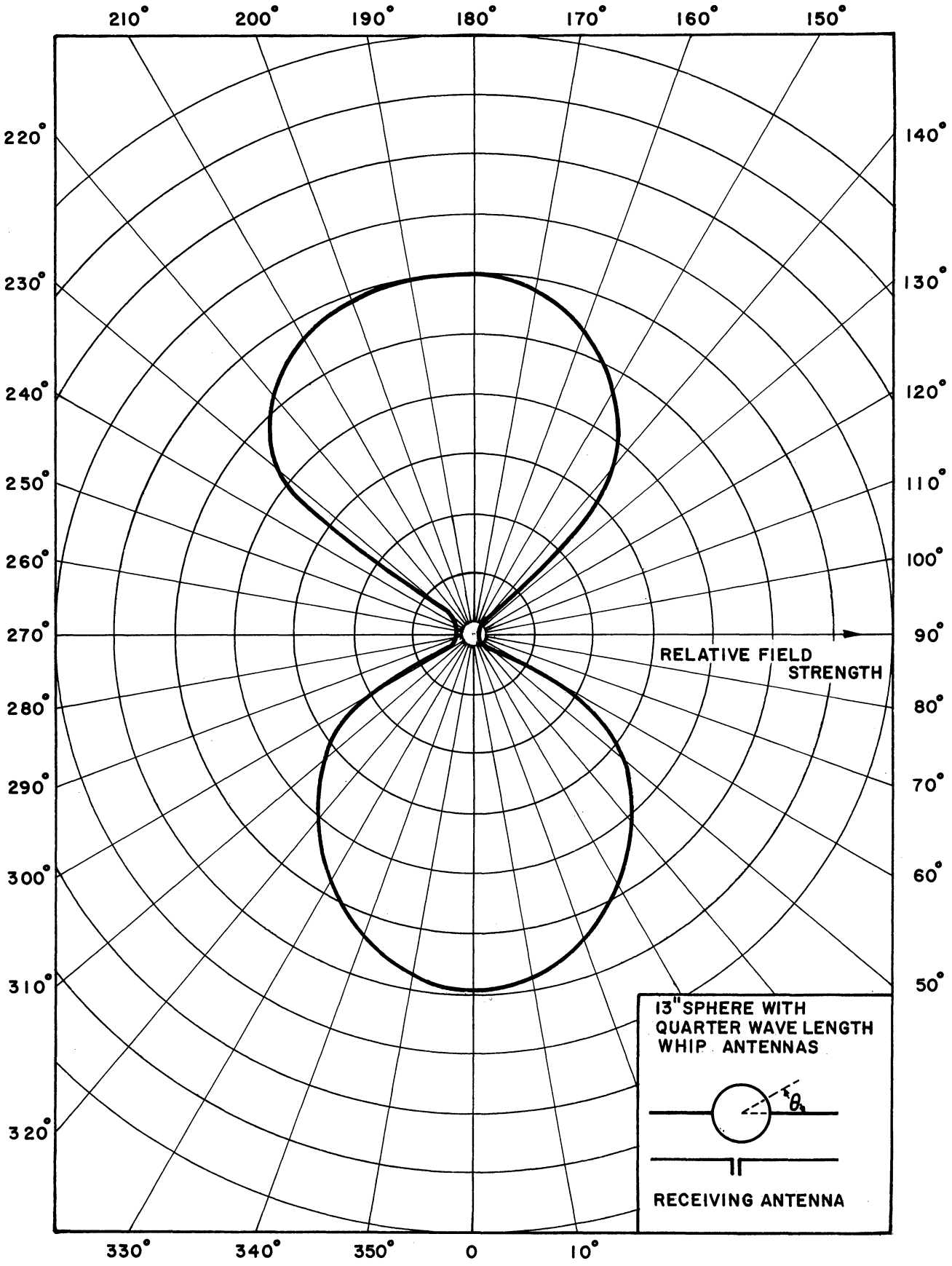

Fig. 26. Radiation pattern of the 13-in. sphere with two quarter wave-length whip antennas.

VI. NOSE CONE

As discussed Section II, the instrument package is to be carried in the rocket under vacuum up to an altitude of about 100 km where it is to be ejected into the atmosphere. The Aerobee 150 nose cone and extension assembly designed for this purpose is shown in Fig. 27 and will now be described in detail.

The nose cone is split into two halves along the longitudinal axis of the cone. The halves are held together, against a spring force of 100 lb, by a frangible ring. This ring is a relieved magnesium O-ring, which is detonated by timer-actuated squibs, permitting the springs to force the halves apart at the required moment. It is designed so that the gases resulting from the explosion are directed away from the instrument package. Two additional springs are placed near the hinges to ensure the complete opening of the nose cone.

The vacuum chamber in which the 13-in.spherical instrument package is carried within the nose cone consists of a hemisphere welded to one of the nose-cone halves and a vacuum-tight compartment mounted in the rocket extension. A Viton O-ring is used to obtain a vacuum seal between these two sections of the vacuum chamber. The flanges of these two sections mate when the nose cone is closed.

The 13-in. sphere rests on a spring-loaded platform. The spring is held under compression by two series-connected explosive bolts, which are timer-actuated. The ejection spring forces the platform upward when either one or both of the bolts are activated. A stainless-steel bellows surrounds the spring to keep the gases, given off by the explosives, out of the vacuum chamber.

A lanyard is employed to impart the necessary angular rotation of approximately 1 cps to the sphere. The platform actuating spring is chosen such that the sphere leaves the platform with a linear velocity V_i of about 4.5 ft/sec. The lanyard exerts a tangential restraining force on the sphere shortly after it has left the platform, transferring a certain portion of the translational energy into rotational energy. Assuming that no energy is transferred into or taken from the lanyard spring, the final linear and angular velocity of the sphere can be determined from Eqs. (7) and (8):

$$\frac{1}{2} MV_i^2 = \frac{1}{2} MV_f^2 + \frac{1}{2} I\omega^2 \tag{7}$$

$$\omega = \frac{V_f}{r} \tag{8}$$

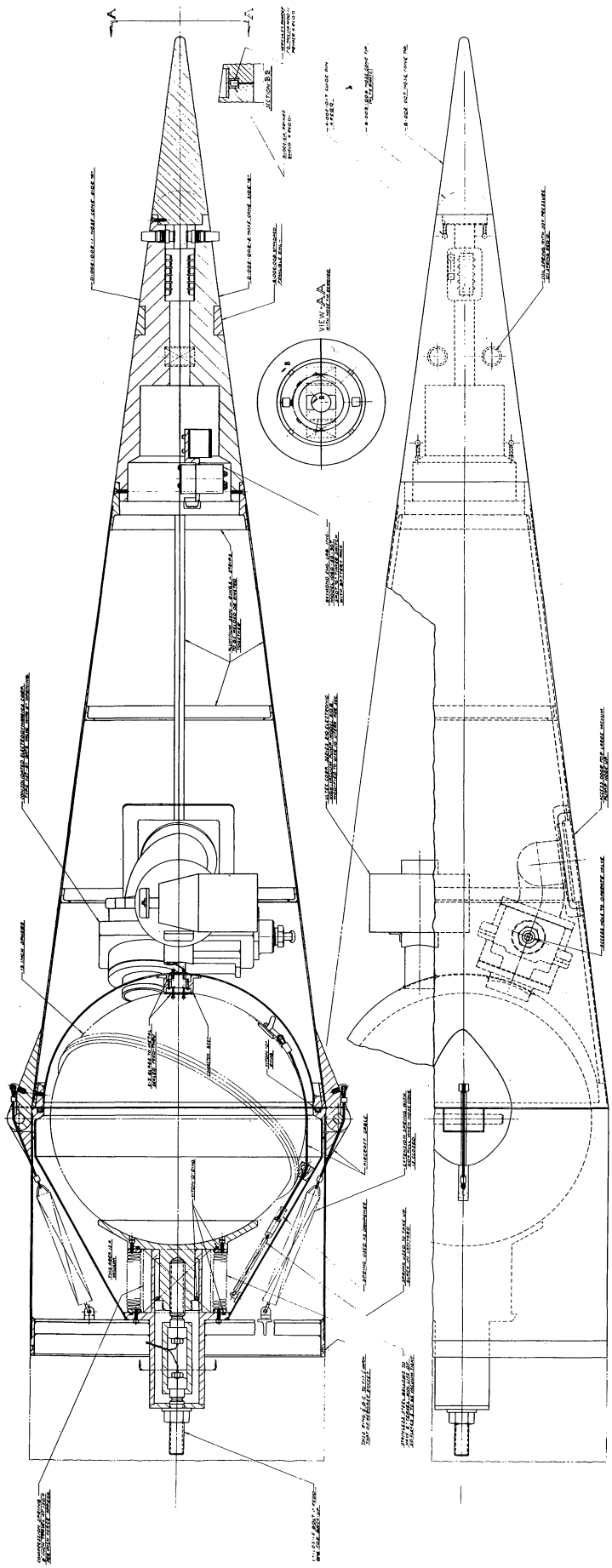

Fig. 27. Details of the nose cone and extension assembly.

where

M = mass of the sphere
I = moment of inertia of the sphere
V_i = velocity at which sphere leaves the platform
V_f = velocity of sphere after the lanyard acted on it
ω = angular velocity of sphere
r = radius of sphere

The 10-liters/sec ion pump with its associated magnet and the high-vacuum, high-conductance valve are placed above the vacuum chamber. As described previously, the valve to the external pumping system will be closed sometime before launching and the external vacuum pump will be removed from the launching area. The internal ion pump will then be turned on (using external power) and will pump until launching, maintaining the vacuum inside the chamber at an acceptable level (less, it is hoped, than 10^{-5} mm Hg).

VII. CONCLUSION

This report has described an experiment which in the opinion of the writers holds great possibilities of very-high-altitude measurements of pressure, density, temperature, and possibly composition. The contracts under which most of the work described herein was carried out have now been completed. This report will constitute a final report for those contracts. It is to be noted that the experiment will be continued under NASA support and carried out in concert with the Goddard Space Flight Center.

VIII. ACKNOWLEDGMENTS

As noted, the work described here has been supported by three different contracts. The authors wish to express their appreciation for the support given by Mr. W. G. Stroud* and the Army Signal Research and Development Laboratory, who made possible the initiation and main support of the effort; Mr. W. W. Berning and the Ballistic Research Laboratory, who also provided a large measure of support for the activity; and Mr. R. Horowitz and the Goddard Space Flight Center, who provided laboratory equipment as well as financial support of the efforts.

The development of an experiment as complex as this obviously represents the ideas and efforts of many people. L. H. Brace has acted as project director since the departure of Professor N. W. Spencer,* now on leave of absence from the University. B. J. Campbell did much of the work on designing the nose-cone assembly and Paul Tibbals helped in designing the mounting fixtures of the sensors.

The early models of the omegatron were built by Robert L. Boyd. During all the omegatron developments program, much assistance was received from personnel of the Electron Tube Laboratory of The University of Michigan, especially from Lynn E. Paul. Major contributors to circuit development, calibration, etc., have been Duane Beechler, Jack Horvath, William Kartlick, John Maurer, Keith McKenna, Joe D. Nelson, and Robert Wallace.

*Now at Goddard Space Flight Center.

APPENDIX I

A body is moving in space with an arbitrary velocity $\vec{V}$ and is carrying a pressure-measuring sensor mounted in a chamber which is connected to the outside atmosphere via a knife edge orifice having a cross-sectional area A. To simplify calculations, let us choose a set of coordinates fixed in space in such a fashion that the positive x-axis points in a direction normal to the orifice. We denote the thermal velocity of the neutral particles by $\vec{U}$ in this coordinate system. The relative velocity between the body and particle is $\vec{W} = \vec{U} - \vec{V}$. Assuming a Maxwellian velocity distribution, we can write

$$\frac{dN}{dU_{ox}dU_{oy}dU_{oz}} = \frac{N_o}{(U_o\sqrt{\pi})^3} \exp\left[-\frac{U_{ox}^2 + U_{oy}^2 + U_{oz}^2}{U_o^2}\right] \tag{9}$$

where

N_o = ambient atmospheric number density
U_o = most probable thermal velocity of the neutral gas particle
$\vec{U}_o$ = thermal velocity of neutral particle
U_{ox} = x component of thermal velocity $\vec{U}_o$
U_{oy} = y component of thermal velocity $\vec{U}_o$
U_{oz} = z component of thermal velocity $\vec{U}_o$

The number of particles entering the chamber through the orifice in time dt is

$$dG_o = \left[\frac{N_o A}{(U_o\sqrt{\pi})^3} \iint \vec{W}\cdot\vec{x} \exp\left(-\frac{U_{ox}^2 + U_{oy}^2 + U_{oz}^2}{U_o^2}\right) dU_{ox}dU_{oy}dU_{oz}\right] dt \tag{10}$$

$$= \left[\frac{N_o A U_o}{\pi^{3/2}} \iint \left(\frac{U_{ox}}{U_o} - \frac{V_x}{U_o}\right) \exp\left(-\frac{U_{ox}^2 + U_{oy}^2 + U_{oz}^2}{U_o^2}\right) \frac{dU_{ox}}{U_o}\frac{dU_{oy}}{U_o}\frac{dU_{oz}}{U_o}\right] dt$$

Let us now define a tangential velocity vector U_t satisfying Eqs. (11) and (12)

$$U_{oy} = U_{ot} \cos\theta \tag{11}$$

$$U_{oz} = U_{ot} \sin\theta \tag{12}$$

Thus we can write

$$dU_{oy}dU_{oz} = U_{ot}dU_{ot}d\theta \tag{13}$$

As θ varies from 0 to 2π, Eq. (10) becomes

$$dG_o = \left[\frac{2N_oAU_o}{\sqrt{\pi}} \iint \frac{U_{ot}}{U_o}\left(\frac{U_{ox}}{U_o} - \frac{V_x}{U_o}\right)\exp\left(-\frac{U_{ox}^2 + U_{ot}^2}{U_o^2}\right)\frac{dU_{ox}}{U_o}\frac{dU_{ot}}{U_o}\right]dt \tag{14}$$

The limits of the integral are

$$-\infty \lesssim U_{ox} < V_x$$

$$0 < U_{ot} < \infty$$

Now let

$$p = \frac{U_{ox}}{U_o} \tag{15}$$

$$r = \frac{U_{ot}}{U_o} \tag{16}$$

$$s = \frac{V_x}{U_o} \tag{17}$$

$$dG_o = \left[\frac{2N_oAU_o}{\sqrt{\pi}} \int_0^{\infty}\int_{V_x}^{-\infty} r(p-s)\exp(-p^2 - r^2)\,dp\,dr\right]dt \tag{18}$$

$$= \frac{N_oAU_o}{2\sqrt{\pi}}\left[e^{-s^2} + \sqrt{\pi}\,s\{1 + \mathrm{erf}(s)\}\right]dt$$

The number of particles leaving the chamber in time dt, assuming Maxwellian velocity distribution, is

$$dG_i = \frac{AN_iU_i}{\sqrt{\pi}}\left[\int_0^{\infty}\frac{U_{ix}}{U_i}\exp\left(-\frac{U_{ix}^2}{U_i^2}\right)\frac{dU_{ix}}{U_i}\,dt\right] = \frac{AN_iU_i}{\sqrt{\pi}} \tag{19}$$

where

U_i = most probable particle velocity inside the chamber
N_i = particle number density inside the chamber

Under equilibrium conditions

$$G_i = G_o \tag{20}$$

$$\frac{N_i U_i}{N_o U_o} = \left[e^{-s^2} + \sqrt{\pi}\, s \{1 + \mathrm{erf}(s)\} \right] \tag{21}$$

Assuming that the gas composition inside the chamber is that of the ambient atmosphere, rearranging the energy Eq. (22) and Eq. (1) will give (23)

$$kT = 1/2\, mU^2 \tag{22}$$

where

k = Boltzman's constant
m = molecular weight

$$\frac{N_i U_i}{N_o U_o} = \frac{P_i}{P_o} \sqrt{\frac{T_o}{T_i}} \tag{23}$$

Substituting (23) into (21), we finally get (2)

$$\frac{P_o}{P_i} = \sqrt{\frac{T_o}{T_i}} \left[e^{-s^2} + \sqrt{\pi}\, s \{1 + \mathrm{erf}(s)\} \right] \tag{2}$$

APPENDIX II

The principle of operation of the omegatron has been covered in great detail in a number of excellent articles; nevertheless, a short review of it will be given here for completeness.

The set of differential equations describing the motion of a charged particle in a crossed electric and magnetic field are Eqs. (24), (25), and (26):

$$\frac{d^2x}{dt^2} = \omega_o \frac{dy}{dt} + \frac{q}{m} E \tag{24}$$

$$\frac{d^2y}{dt^2} = - \omega_o \frac{dx}{dt} \tag{25}$$

$$\frac{d^2z}{dt^2} = 0 \tag{26}$$

where

ω_o = qB/m
q = electronic charge
m = mass of particle
B = magnetic flux density
E = electric field

Let us assume that the charged particle at t = 0 has an initial velocity v_o and is at x = y = z = 0. It follows from Eq. (26) that its movement in the z direction is simply

$$z = v_{zo}t$$

where

v_{xo} = initial velocity of charged particle in the x direction.
v_{yo} = initial velocity of charged particle in the y direction.
v_{zo} = initial velocity of charged particle in the z direction.

Assuming a uniform alternating electric field E sin ωt, the motion of the particle in the x-y plane can be found by combining and solving Eqs. (24) and (25). The solution to these equations should be separated into two different cases, the resonant and the nonresonant, that is, when the angular velocity of the applied electric field is equal or not equal to ω_o, respectively.

The use of complex notation for simplicity in writing the results was suggested by Berry,[8] and Eq. (27) gives the solution for the trajectory in that form, for the nonresonant case.

$$x + iy = i\frac{v_o^*}{\omega_o}\left\{\exp\left[-i\omega_o(t-\phi/\omega)\right] - 1\right\} - i\frac{\alpha}{\omega^2-\omega_o^2}\left[\frac{\omega_o}{\omega}\cos\omega t - i\sin\omega t\right] \tag{27}$$

$$+ i\frac{\alpha}{\omega^2-\omega_o^2}\left[\frac{\omega}{\omega_o}\cos\phi - i\sin\phi\right]\exp\left[-i\omega_o(t-\phi/\omega)\right] - i\frac{\alpha}{\omega_o\omega}\cos\phi$$

where

v_o^* = $v_{xo} + iv_{yo}$

i = $\sqrt{-1}$

α = qE/m

ϕ = the phase angle relating the time of origin of a particle to the phase of the applied field.

All the terms in this equation are either periodic or constant; hence the maximum amplitude of the motion is closely bounded.

To get the orbit described by a resonant ion, we take the limit as $\omega \to \omega_o$ of Eq. (27), which after some simplification, gives (28):

$$x + iy\Big|_{\omega=\omega_o} = \left(\frac{iv_o^*}{\omega_o}\right)\left\{\exp\left[-i\omega_o(t-\phi/\omega_o)\right] - 1\right\} \tag{28}$$

$$- \left(\frac{\alpha}{2\omega_o^2}\right)\left\{\omega_o t - \phi - i\left[\exp(i\phi)\right]\cos\phi\right\}\exp\left[-i\omega_o t\right] + \frac{i\alpha}{2\omega_o^2}(\cos\omega_o t) - \frac{i\alpha}{\omega_o^2}(\cos\phi)$$

The second term is the most important one in Eq. (28) because after a few cycles all the other terms become negligible compared to it, that is, the motion of the particle in resonance closely approaches an Archimedes spiral. This approximation gives (29).

$$r \approx \frac{t\,E_o}{2B} \tag{29}$$

From Eq. (27) we get the following approximate relationship for frequencies slightly off resonance:

$$r \approx \frac{E}{B\epsilon}\sin\frac{\epsilon t}{2} \tag{30}$$

where

$$\epsilon = \omega - \omega_o$$

If the collector is placed at $r = R_o$, then the nonresonant ions will not reach it, if condition (31) is satisfied.

$$\frac{E}{B\epsilon} < R_o \tag{31}$$

The kinetic energy W_k of the ions at the moment of collection is given by Eq. (32)

$$W_k = \frac{1}{2} m v_t^2 = \frac{1}{2} m \omega_o^2 R_o^2 = \frac{q^2 B^2 R_o^2}{2m} = \frac{q^2 E_o^2 t^2}{8m} \tag{32}$$

It is often desirable to know the total path length of the ion to compare it with the mean free path. The length (L) of an Archimedes spiral is approximately the number of revolutions (n) times the mean radius. Hence for a collector placed at R_o we get (33):

$$L = \pi n R_o \tag{33}$$

The resolution of the omegatron is defined by:

$$\text{resolution} = \gamma = \frac{m}{\Delta m} = \frac{\omega_o}{2\epsilon^*} \tag{34}$$

where

$$2\epsilon^* = \frac{2E}{BR_o} = \text{frequency width of the base of the resonant peak} \tag{35}$$

Combining (34) and (35), we get Eq. (36)

$$\gamma = \frac{qB^2 R_o^2}{2Em} \tag{36}$$

The trapping potentials, which are used to stop the resonant ions from drifting out of the action volume before they would be collected, as well

as the ionizing electron beam will create a radial electric field, which changes the cyclotron resonant frequency. It has been shown[17] that the resonant frequency with a superimposed radial electric field is given by (37) if E_r/r is small and independent of r:

$$\omega_{or} = \frac{qB}{m} - \frac{E_r}{Br} \tag{37}$$

where

E_r/r = ratio of the radial component of the perturbing electric fields to the radius of the orbit of the cycling ion.

ω_{or} = modified resonant frequency.

REFERENCES

1. Spencer, N. W., Boggess, R. L., LaGow, H. E., and Horowitz, R., "On the Use of Ionization Gage Devices at Very High Altitude," American Rocket Society Journal, 29:290-94 (1959).

2. Dow, W. G., and Reifman, A., Technical Report on the Measurement of Temperature and Pressure in the Ionosphere, Univ. of Mich. Eng. Res. Inst. Report, Ann Arbor, July, 1946.

3. Schultz, F. V., Spencer, N. W., and Reifman, A., Atmospheric Pressure and Temperature Measurement Between the Altitudes of 40 and 110 Kilometers, Upper-Air Research Program Report No. 2, Univ. of Mich. Eng. Res. Inst. Report, Ann Arbor, July, 1948.

4. Horowitz, R., and LaGow, H. E., "Upper Air Pressure and Density Measurements from 90 to 220 Kilometers with the Viking 7 Rocket," Journal of Geophysical Research, 62:57-78 (1957).

5. Danilin, B. S., Mikhnevich, V. V., Repnev, A. I., and Shvidkovskii, E. G., "The Problem of Pressure and Density Measurements in the Upper Atmospheric Layers by means of an Artificial Earth Satellite," The Russian Literature of Satellites, Part II (International Physical Index, Inc., New York, 1958), pp. 95-117.

6. Horowitz, R., and LaGow, H. E., "Summer-Day Auroral-Zone Atmospheric-Structure Measurements from 100 to 210 Kilometers," Journal of Geophysical Research, 63:757-73 (1958).

7. Horowitz, R., LaGow, H. E., and Guiliani, J. F., "Fall-Day Auroral-Zone Atmospheric Structure Measurements from 100 to 188 Km," Journal of Geophysical Research, 64:2287-95 (1959).

8. Hipple, J. A., Sommer, H., and Thomas, H. A., "A Precise Method of Determining the Faraday by Magnetic Resonance," Physical Review, 76:1877-78 (1949).

9. Sommer, H., Thomas, H. A., and Hipple, J. A., "Measurement of e/m by Cyclotron Resonance, Physical Review, 82:697-702 (1951).

10. Berry, C. E., "Ion Trajectories of the Omegatron," Journal of Applied Physics, 25:28-31 (1954).

11. Warnecke, R. J., "Etude et Realisation d'un Spectrometre de masse du Type Omegatron," Extrait des Annales de Radio electricite, 14, No. 58 (1959) and 15, No. 60 (1960).

12. Sommer, H., and Thomas, H. A., "Detection of Magnetic Resonance for Ion Resonance Absorption," Physical Review, 78:806 (1950).

13. Nagy, A. F., Research on the Use of Electronic and Mechanical Apparatus and Instrumentation for Rockets and Satellites, O.R.A. Quarterly Status Report, in preparation.

14. Alpert, D., "New Developments in the Production and Measurements of Ultra High Vacuum," Journal of Applied Physics, 24:860-76 (1953).

15. Horvath, J., Radioactive Sensitive Measuring System, O.R.A. 3554-HS-2, in preparation.

16. Matzen, W. T., and Baird, J. R., "Differential Amplifier Features D.C. Stability," Electronics, 32:60-63 (1959).

17. Woodford, H. J., and Gardner, J. H., "Method for Eliminating Omegatron Radial Field Errors or for Direct Measurement pf Mass Ratios," The Review of Scientific Instruments, 27:378-81 (1956).